Molecular Microbiology (2016) 102(4), 642–671 ■
doi:10.1111/mmi.13484
First published online 7 October 2016

The *Aspergillus fumigatus* SchA^{SCH9} kinase modulates SakA^{HOG1} MAP kinase activity and it is essential for virulence

Patrícia Alves de Castro,[1] Thaila Fernanda dos Reis,[1] Stephen K. Dolan,[2] Adriana Oliveira Manfiolli,[1] Neil Andrew Brown,[3] Gary W. Jones,[2] Sean Doyle,[2] Diego M. Riaño-Pachón,[4] Fábio Márcio Squina,[4] Camila Caldana,[4,5] Ashutosh Singh,[6] Maurizio Del Poeta,[6] Daisuke Hagiwara,[7] Rafael Silva-Rocha[8] and Gustavo H. Goldman[1]*

[1]*Faculdade de Ciências Farmacêuticas de Ribeirão Preto, Universidade de São Paulo, Ribeirão Preto, Brazil.*
[2]*Department of Biology, Maynooth University, Maynooth, Co. Kildare, Ireland.*
[3]*Plant Biology and Crop Science, Rothamsted Research, Harpenden, Herts AL5 2JQ, UK.*
[4]*Laboratório Nacional de Ciência e Tecnologia do Bioetanol (CTBE), Centro Nacional de Pesquisa em Energia e Materiais (CNPEM), Caixa Postal 6192, Campinas, São Paulo, CEP 13083-970, Brasil.*
[5]*Max Planck Partner Group at Brazilian Bioethanol Science and Technology Laboratory, Brazilian Center for Research in Energy and Materials, São Paulo, Brazil.*
[6]*Department of Molecular Genetics and Microbiology, Stony Brook University, Stony Brook, NY, USA.*
[7]*Medical Mycology Research Center, Chiba University, Chiba, Japan.*
[8]*Faculdade de Medicina de Ribeirão Preto, Universidade de São Paulo, Ribeirão Preto, Brazil.*

Summary

The serine-threonine kinase TOR, the Target of Rapamycin, is an important regulator of nutrient, energy and stress signaling in eukaryotes. Sch9, a Ser/Thr kinase of AGC family (the cAMP-dependent PKA, cGMP- dependent protein kinase G and phospholipid-dependent protein kinase C family), is a substrate of TOR. Here, we characterized the fungal opportunistic pathogen *Aspergillus fumigatus* Sch9 homologue (SchA). The *schA* null mutant was sensitive to rapamycin, high concentrations of calcium, hyperosmotic stress and SchA was involved in iron metabolism. The Δ*schA* null mutant showed increased phosphorylation of SakA, the *A. fumigatus* Hog1 homologue. The *schA* null mutant has increased and decreased trehalose and glycerol accumulation, respectively, suggesting SchA performs different roles for glycerol and trehalose accumulation during osmotic stress. The *schA* was transcriptionally regulated by osmotic stress and this response was dependent on SakA and MpkC. The double Δ*schA* Δ*sakA* and Δ*schA* Δ*mpkC* mutants were more sensitive to osmotic stress than the corresponding parental strains. Transcriptomics and proteomics identified direct and indirect targets of SchA post-exposure to hyperosmotic stress. Finally, Δ*schA* was avirulent in a low dose murine infection model. Our results suggest there is a complex network of interactions amongst the *A. fumigatus* TOR, SakA and SchA pathways.

Accepted 17 August, 2016. *For correspondence. E-mail ggoldman@usp.br; Tel. 55-16-36024280/81; Fax 55-16-6331092.

Introduction

A central coordinator of nutrient, energy and stress signaling in eukaryotes is the highly conserved protein serine-threonine kinase TOR, the Target of Rapamycin that belongs to the phosphatidylinositol kinase-related (PIKK) family (Wullschleger *et al.*, 2006; Laplante and Sabatini, 2012; Robaglia *et al.*, 2012; Cornu *et al.*, 2013; Dobrenel *et al.*, 2013; Yuan *et al.*, 2013). Rapamycin is a macrocyclic lactone produced by *Streptomyces hygroscopicus* that inhibits proliferation and has potent immunosuppressive properties (Wullschleger *et al.*, 2006). TOR was identified for the first time in *Saccharomyces cerevisiae* through genetic mutant screens for resistance to rapamycin (Heitman *et al.*, 1991). TOR supports cell growth in response to nutrients, growth factors and cellular energy, by repressing catabolic

processes (such as mRNA degradation, ubiquitin-dependent proteolysis, autophagy or apoptosis) and activating anabolic processes (such as nutrient transport, ribosome biogenesis, protein synthesis, or mitochondrial metabolism; Liko and Hall, 2015). Two TOR genes have been identified in *S. cerevisiae*. However, only one TOR gene is found in plants, animals and filamentous fungi (Wullschleger *et al*., 2006; Liko and Hall, 2015). TOR exists as two multi-protein complexes, TOR complex 1 (TORC1) and TOR complex 2 (TORC2), which are found both in animals and in yeast (Wullschleger *et al*., 2006). Yeast TORC1 regulates protein synthesis, ribosome biogenesis, translation, nutrient uptake or autophagy and is sensitive to rapamycin while TORC2 regulates actin organization, lipid synthesis and cell survival and is not sensitive to rapamycin (Loewith *et al*., 2002; Reinke *et al*., 2004; Wullschleger *et al*., 2006). In filamentous fungi, very little is known about the mechanism and function of TOR signaling. Model filamentous fungi such as *Aspergillus nidulans*, *A. fumigatus*, *Fusarium graminearum* and *Podospora anserina* are sensitive to rapamycin (Fitzgibbon *et al*., 2005; Teichert *et al*., 2006; Lopez-Berges *et al*., 2010; Yu *et al*., 2014; Baldin *et al*., 2015). Recently, Baldin *et al*. (2015) showed that in *A. fumigatus* TOR participates in the regulation of ornithine biosynthesis, a major precursor of siderophores, iron-chelating molecules that are important for adaptation to iron starvation and virulence.

S. cerevisiae Sch9p is a Ser/Thr kinase of the AGC family (the cAMP-dependent PKA, cGMP-dependent protein kinase G and phospholipid-dependent protein kinase C family) and a substrate of TORC1. Sch9p is directly phosphorylated by TORC1, while rapamycin or nutrient starvation inhibits this phosphorylation (Urban *et al*., 2007). Sch9 regulates ribosome biogenesis, adaptation to nutrient availability and aging (Powers, 2007). Sch9 regulates ribosome biosynthesis similarly to the mammalian S6K1, responding to nutrient resources and aging (Fabrizio *et al*., 2001; Jorgensen *et al*., 2004). Recently, González *et al*. (2015) have shown, using a highly specific antibody that recognizes phosphorylation of TORC1 target ribosomal protein S6 (Rps6), that in *S. cerevisiae* nutrients rapidly induce Rps6 phosphorylation in a TORC1-dependent manner. However, these authors demonstrated that Sch9p is dispensable for Rps6 phosphorylation.

Pascual-Ahuir and Proft (2007) have described a novel role for *S. cerevisiae* Sch9p in the transcriptional activation of osmostress-inducible genes and observed that the *sch9* mutant was sensitive to hyperosmotic stress. During osmotic stress, the mutant showed reduced expression of genes important for osmotic shock adaptation, among them the transcription factor Sko1p, which is directly targeted by the mitogen-activated protein (MAP) kinase, Hog1. Interestingly, *in vitro*, Sch9p interacts with both Sko1p and Hog1p, and phosphorylates Sko1p. Hog1p is the main regulator of the high osmolarity glycerol response (HOG) pathway (Maeda *et al*., 1994). This raised the interesting hypothesis that Sch9p might act as an intermediary for the crosstalk between TOR and HOG pathways. Accordingly, in the filamentous phytopathogen *F. graminearum*, the Δ*FgSch9* mutant exhibited increased sensitivity to osmotic and oxidative stress, cell wall-damaging agents and rapamycin, while showing increased thermal tolerance (Chen *et al*., 2014; Gu *et al*., 2015). In addition, co-immunoprecipitation and affinity capture-mass spectrometry showed that FgSch9 interacted with FgTOR and FgHog1. In other filamentous fungi, Sch9 homologues have also been linked to interconnecting various stress responses and signaling pathways. In the hypercellulolytic fungus *Trichoderma reesei*, the *Trsch9*Δ mutant displayed a decreased growth rate on different carbon sources, produced less conidia and cellulase, while having defects in the cell wall integrity pathway (Lv *et al*., 2015). *A. nidulans* strain defective for SchA showed altered trehalose mobilization and kinetics of germ tube outgrowth, in addition to other defects in colony formation (Fillinger *et al*., 2002). *A. nidulans schA* null mutant also showed a dramatic reduction in the cellulose-induced transcriptional responses, including the expression of hydrolytic enzymes and transporters, due to an inability to unlock CreA-mediated carbon catabolite repression under derepressing conditions (Brown *et al*., 2013).

A. fumigatus is a ubiquitous air-borne saprophytic fungus, found living on decaying organic and plant materials (de Vries and Visser, 2001; Tekaia and Latgé, 2005; Kwon-Chung and Sugui, 2013). This major opportunistic allergenic fungus causes a significant percentage of all invasive fungal infections in humans and is the most common cause of fungal pulmonary infections in mammals (Greenberger, 2002; Dagenais and Keller, 2009; Brown *et al*., 2012a,b; Lackner and Lass-Flörl, 2013). *A. fumigatus* causes several clinical diseases including the life-threatening disease, invasive pulmonary aspergillosis (IA) that has high mortality with fatality rates reaching 80% in neutropenic patients (Brown *et al*., 2012a, 2012b; Lackner and Lass-Flörl, 2013). Calcium signaling plays an important role in *A. fumigatus* virulence (Thewes, 2014). The *A. fumigatus* transcription factor CrzA regulates calcium signaling and we have shown by ChIP-seq (Chromatin Immunoprecipitation DNA sequencing) its putative gene targets (de Castro *et al*., 2014). Some of these targets are for instance the PhkB histidine kinase and the SskB MAP kinase kinase kinase of the HOG pathway. Additionally, we were able to show that CrzA::GFP goes to the nucleus during

osmotic stress (de Castro *et al*., 2014). Phosphorylation of the SakA^{HOG1} MAPK is dependent on CrzA in response to osmotic stress. Taken together, these results strongly suggest an interaction between *A. fumigatus* calcium-calcineurin-CrzA and HOG pathways. One of the gene targets identified in this screening was the Sch9 homologue, named SchA. Here, we show that Δ*schA* mutation was more sensitive to rapamycin, high concentrations of calcium and hyperosmotic stress, while SchA is involved in iron metabolism. The *schA* null mutant showed increased SakA phosphorylation. Transcriptomics and proteomics identified direct or indirect targets of SchA during hyperosmotic stress. Finally, Δ*schA* was avirulent in a low dose murine infection model. Our results show the complex network of interactions between CrzA, SakA, TOR and SchA pathways.

Results

The ΔschA *mutant is more sensitive to calcium and osmotic stress*

A BLASTp search of the *A. fumigatus* genome revealed a single putative orthologue of the *S. cerevisiae* Sch9, Afu1g06400 (named SchA). The *schA* gene model is supported by RNA-seq data (available at www.aspgd.org) and the hypothetical protein is predicted to be 934 amino acids in length and possess a mass of 102.8 kDa. *A. fumigatus* SchA has 66.1% identity and 78.8% similarity with *S. cerevisiae* Sch9p over their best local alignment (e value = 2e-180; BLASTp alignment) and 37.2% and 47.2% globally (Needleman-Wunsch global alignment). A comparison of protein structure and organization between Sch9 and SchA was performed using the SMART interface (http://smart.embl-heidelberg.de/). Similar to Sch9, the orthologous SchA protein in *A. fumigatus* was predicted to contain a protein kinase C conserved region 2 (CalB, SM000239), a serine/threonine protein kinase catalytic domain (SM000220) and an extension to Ser/Thr-type protein kinases (SM000133) (Supporting Information Fig. S1). *S. cerevisiae* Sch9 is phosphorylated by Pkh1/2 at Thr570 residue (Voordeckers *et al*., 2011), which is conserved in SchA (Thr696) and by TORC1 kinases at residues Ser711, Thr723, Ser726, Thr737, Ser758, Ser 765, of which three are conserved in SchA (Thr857, Ser860, Thr871) (Supporting Information Fig. S1).

To gain an initial insight into the function of the Sch9 homologue in *A. fumigatus*, a *schA* null mutant and complemented strains were generated (Supporting Information Fig. S2). The wild-type, Δ*schA* and Δ*schA*::*schA*$^{+}$ strains were grown in minimal medium (MM) and exposed to agents that affect calcineurin-CrzA signaling, including $CaCl_2$ and $MnCl_2$ (Soriani *et al*., 2008), and those that induce osmotic stress such as NaCl and sorbitol (Fig. 1A–C). The Δ*schA* strain showed radial growth and conidiation similar to the wild-type strain (data not shown). The Δ*schA* was more susceptible to $CaCl_2$, $MnCl_2$ and osmotic stress (Fig. 1A–C). The Δ*schA* strain was slightly more sensitive to the phenylpyrrole antifungal agent fludioxonil, but showed the same sensitivity as the wild-type strain to antifungal dicarboximide iprodione, azoles and echinocandin, itraconazole and caspofungin (Supporting Information Fig. S3; data not shown).

Schizosaccharomyces pombe Sch9 directly phosphorylates Rps6 when TOR is active (Nakashima *et al*., 2010). Therefore in *A. fumigatus* SchA activity was measured by quantifying the phosphorylation of the ribosomal protein S6 (Rps6), a well-known downstream target of SchA orthologues, using immunoblot analysis with a commercial phospho-specific antibody against Ser235 and Ser236 of human Rps6, which has already been shown as able to recognize Rps6 phosphorylated residues in *S. pombe* and *S. cerevisiae* homologues (Nakashima *et al*., 2010; González *et al*., 2015). The phosphorylated serines with an arginine (R) or a lysine (K) at position −4 (relative to phosphorylated serine) which are recognized by this antibody are conserved in *A. fumigatus* (data not shown). Negative and a positive controls of Rps6A-P from MCF7 cell lines not induced (C-) or induced with insulin (C+) showed that the Rps6-P antibody is functional (data not shown). In both the wild-type and Δ*schA* strains, the total Rps6 concentration is constant with rapamycin and decreases with time in the presence of sorbitol (Fig. 1D and E). We have evaluated the RPS6-P/total RPS6 signal by densitometric analysis by using the ImageJ software (http://rsbweb.nih.gov/ij/index.html). Post exposure to 30 and 60 min rapamycin, the wild-type strain displayed an 80 and 50% decrease in the Rps6-P/Rps6 ratio, while the Δ*schA* mutant showed an 80 and 96% decrease (Fig. 1D). Upon osmotic stress, the total concentration of Rps6 was about 30% decreased in the wild-type strain, while the Δ*schA* mutant showed a 40–55% decrease (Fig. 1E). In addition, the Rps6-P/Rps6 ratio showed a 30 and 80% decrease in the wild-type strain, while the Δ*schA* mutant displayed an 80 and 95% decrease, when compared to the control (Fig. 1E). These results suggest that SchA is important for Rps6A phosphorylation and stability, the latter, when *A. fumigatus* is subject to osmotic stress.

In accordance with a role in TOR signaling, the Δ*schA* mutant displayed slightly increased sensitivity to rapamycin (Fig. 2), and this sensitivity was not increased during osmotic stress (data not shown). The complemented Δ*schA::schA*$^{+}$ strain showed the same

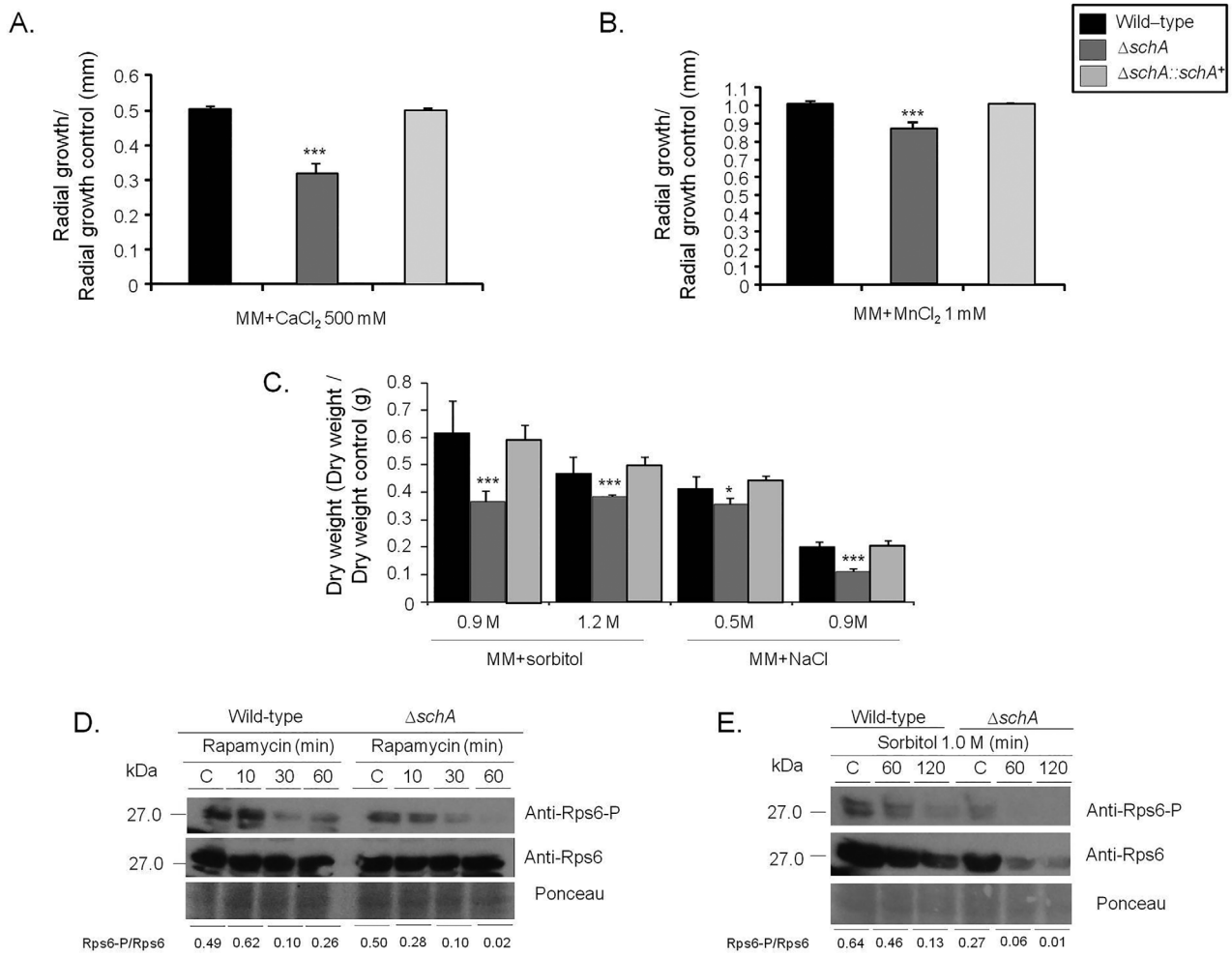

Fig. 1. The *A. fumigatus* Δ*schA* mutant is more sensitive to osmotic stress and increased calcium concentrations.
A and B. Radial Growth of the *A. fumigatus* wild-type, Δ*schA*, and Δ*schA::schA*$^{+}$ on MM, MM + $CaCl_2$ 500 mM or MM + $MnCl_2$ 1 mM. The data are expressed as radial growth sorbitol/radial growth control (mm).
C. The strains were inoculated in liquid MM with increasing concentrations of sorbitol or NaCl and incubated with agitation for 48 h at 37°C. The data are expressed as dry weight sorbitol/dry weight control (g). The radial diameter and dry weight data are expressed as average ± standard deviation of three independent biological repetitions (* and *** denote $p < 0.01$ and 0.001, respectively, by *t*-tests when compared to the wild-type strain).
D and E. Western blot analysis for the total protein level and phosphorylation state of Rps6. The wild-type and Δ*schA* strains were grown for 16 h at 37°C and exposed, or not, to rapamycin or osmotic stress. Proteins were normalized by Ponceau red staining. Signal intensities were quantified using the Image J software by dividing the intensity of SakA-P/SakA ratio and expressed as fold increase from the control (0 min).

phenotypes as the wild-type strain, strongly indicating that the observed null phenotypes were due to the loss of SchA function (Figs. 1–10 and 11). Taken together, these results show that SchA is more sensitive to rapamycin and is involved in osmotic stress.

SchA null mutant has an increased high-osmolarity glycerol response (HOG)

To determine if Δ*schA* was involved in the HOG pathway in *A. fumigatus*, the amount and phosphorylation state of the Hog1p homologue, SakA, was determined in the presence and absence of osmotic stress. The phosphorylation level of the SakA protein was determined using the anti-phospho-p38 MAPK (Thr180/Tyr182) and anti-Hog1 (y-215) antibodies.

We have previously shown in a time course kinetics (10–60 min exposure to 1 M sorbitol) that 10 min is the timepoint with the highest SakA phosphorylation when *A. fumigatus* is exposed to 1 M sorbitol (Hagiwara *et al.*, 2013). The reduction of SakA phosphorylation in the wild-type strain after 10 min is due to SakA modulation by dephosphorylation by SakA phosphatases (Winkelströter *et al.*, 2015). The Δ*schA* mutant has increased levels of SakA phosphorylation upon osmotic stress (Fig. 3A). However, after longer exposure to

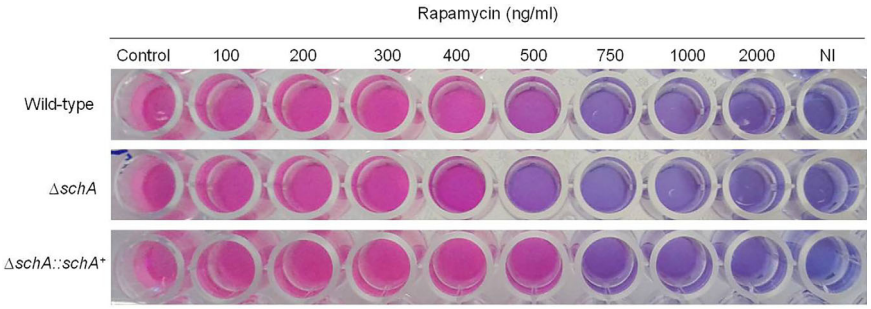

Fig. 2. *A. fumigatus* Δ*schA* is more sensitive to rapamycin. The strains were inoculated in YG medium + Alamar Blue with increasing concentrations of rapamycin, and incubated for 48 h at 37°C. This experiment was repeated three times and the experiment that is shown here is is a representative experiment.

sorbitol, SakA phosphorylation was increased in the Δ*schA* mutant (Fig. 3A). The markers used to evaluate the induction of the HOG pathway include *catA* (catalase, Afu6g03890), *dprA* (dehydrin, Afu4g00860) and *dprB* (dehydrin, Afu6g12180) expression. Catalase and dehydrin-like proteins play a role in oxidative, osmotic and pH stress responses and their expression is dependent on the SakA pathway (Wong Sak Hoi *et al.*, 2011). Upon 1 h osmotic stress, both the wild-type and Δ*schA* mutant showed high levels of *catA*, *dprA* and *dprB* expression that drop after 2–4 h (Fig. 3B). However, in all time points the *catA*, *dprA* and *dprB* mRNA levels are much higher in the Δ*schA* mutant than in the wild-type strain (Fig. 3B). Taken together, these results suggest that SchA influences the HOG pathway in *A. fumigatus*.

Increased levels of glycerol and trehalose are well-known mechanisms to adapt to high osmotic pressure in *S. cerevisiae* and *A. fumigatus* primarily triggered by the HOG pathway (Saito and Posas, 2012; Hagiwara *et al.*, 2014). Subsequently, we studied glycerol production of hyphae in response to 1 M Sorbitol for either 0, 10 min, 30 min, 1, 2 or 4 h (Supporting Information Fig. S4 and Fig. 4C). Upon hypertonic stress from 10 to 60 min or 1 to 4 h the wild-type and Δ*schA::schA*$^{+}$ strains showed a significant increase in glycerol content, while the Δ*schA* mutant strain does not increase as much as the wild type (Supporting Information Fig. S4 and Fig. 3C). Trehalose accumulation in response to 1 M Sorbitol for either 0, 10, 30 or 60 min was also investigated (Fig. 3D). Post hypertonic stress for 10–60 min, the Δ*schA* strain showed significantly increased trehalose levels (Fig. 3D). These results suggest that SchA performs different roles for glycerol and trehalose accumulation during osmotic stress.

SchA genetically interacts with SakA and MpkC MAP kinases upon osmotic stress

Our results indicate that *schA* genetically interacts with *sakA* upon osmotic stress. In *A. fumigatus* SakA and its paralogue MpkC, are involved in osmotic stress, carbon and nitrogen starvation and regulation of conidial germination (May, 2008). In the wild-type strain, *schA* mRNA levels increased post exposure to osmotic stress (Fig. 4). In contrast, no *schA* mRNA accumulation was observed in the Δ*sakA* and the double Δ*mpkC* Δ*sakA* mutants upon osmotic stress (Fig. 4). Interestingly, the Δ*mpkC* mutant showed a higher level of *schA* mRNA accumulation than the wild-type strain (Fig. 4). Our results indicate *schA* was transcriptionally regulated by osmotic stress and that this response was dependent on SakA and MpkC. Highlighting the genetic interaction, the double Δ*schA* Δ*sakA* and Δ*schA* Δ*mpkC* mutants were more sensitive to osmotic stress than the corresponding parental strains (Fig. 5). Additionally, Δ*mpkC* and Δ*sakA* Δ*mpkC* showed increased sensitivity to rapamycin, which also suggested an interaction between TOR and SakA/MpkC pathways (Fig. 6). However, the Δ*schA* Δ*sakA* and Δ*schA* Δ*mpkC* mutants were as sensitive to rapamycin as Δ*schA* (data not shown). It can be emphasized that Δ*schA* did not show sensitivity to 0.9 M sorbitol in solid medium but it did only in liquid medium (compare Figs. 5B to 1C). Interestingly, we were able to see significant differences among *schA* and *sakA* mutants only when we performed experiments by using radial growth but not dry weight measurements. Together, these results suggest SchA and SakA/MpkC interact and both pathways are interacting with TOR.

MpkC::GFP and SakA::GFP are translocated to the nucleus upon osmotic stress with SakA::GFP showing a quicker response (10 min compared to 120 min) (Bruder Nascimento *et al.*, 2016). Accordingly, SakA::GFP migrates to the nucleus after 30 min exposure to Sorbitol 1.0 M, while MpkC::GFP did not (Fig. 7A). Both MpkC::GFP and SakA::GFP do not translocate to the nucleus upon exposure to rapamycin (Fig. 7B). Interestingly, MpkC::GFP translocation for the nucleus is induced after 30 min concomitant exposure to sorbitol and rapamycin (Fig. 7C). These results suggest that TOR modulates the MpkC translocation to the nucleus upon osmotic stress.

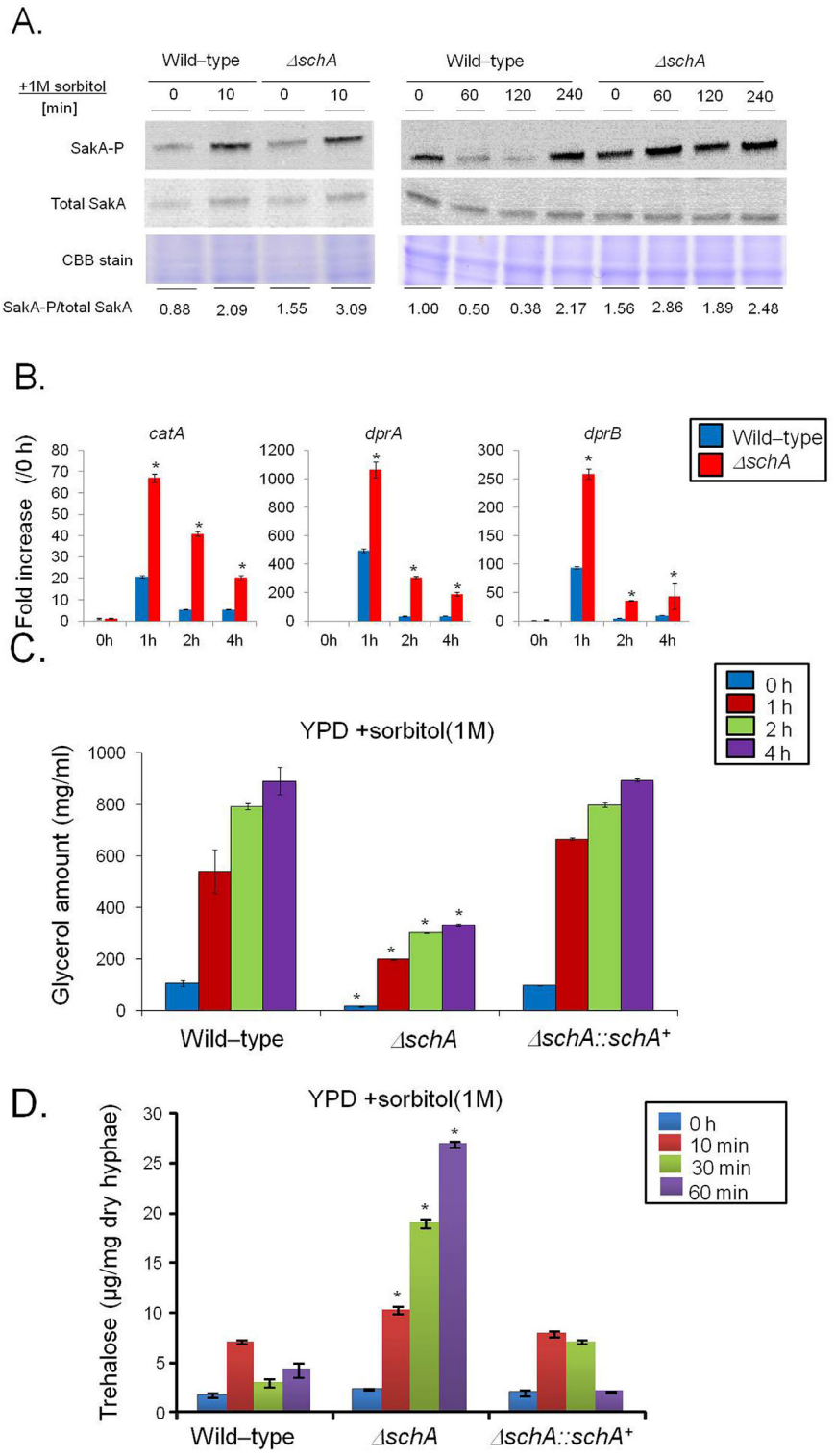

Fig. 3. The *schA* null mutant has increased SakA phosphorylation.
A. Immunoblot analysis for SakA phosphorylation in response to osmotic stress. The wild-type and the *schA* null mutant were grown for 18 h at 37°C. Then, sorbitol (1 M final concentration) was not added (control) and added for 0 (control), 10, 60, 120 and 240 min. The mycelium was harvested at the indicated times, and total proteins were extracted. Anti-phospho-p38 was used to detect the phosphorylation of SakA, and anti-Hog1p was used to detect the total SakA protein. A Coomassie Brilliant Blue (CBB)-stained gel is shown as a loading control. Signal intensities were quantified using the Image J software by dividing the intensity of SakA-P/SakA ratio and expressed as fold increase from the control (0 min).
B. The Δ*schA* mutant shows higher expression of osmostress dependent genes. The wild-type and the Δ*schA* mutant were grown for 18 h at 37°C. Then, sorbitol (1 M final concentration) was added for 0 (control), 1, 2 and 4 h. The mycelium was harvested at the indicated times, and total RNA was extracted. The absolute quantitation of *catA*, *dprA*, and *dprB* and *actA* (Afu6g04740, encoding the actin) was determined by a standard curve (i.e., C_T –values plotted against a logarithm of the DNA copy number). The results are the means (± standard deviation) of four biological replicates (*, $p < 0.001$, comparison of the treatments with wild−type).
C and D. Glycerol and trehalose accumulation in the wild-type, Δ*schA*, and Δ*schA::schA*$^+$ strains upon osmotic stress. The strains were grown for 18 h at 37°C. Then, sorbitol (1 M final concentration) was added for 0 (control), 1, 2 and 4 h. Glycerol and trehalose were quantified and normalized according to the volume of the lysate or dry weight respectively. The results are the means (± standard deviation) of three biological replicates (*, $p < 0.001$, comparison of the treatments with wild-type).

SchA is important for sphingolipid biosynthesis upon osmotic stress

In *S. cerevisiae* Sch9 is an effector of sphingolipid signaling (Spincemaille *et al.*, 2014; Swinnen *et al.*, 2014a, 2014b). Subsequently, we examined sensitivity to sphingolipid inhibitors and the total concentration of different sphingolipids (Fig. 8A; Supporting Information Fig. S5). The Δ*schA* mutant was as sensitive to myriocin (that inhibits serine palmitoyltransferase, the first step in sphingosine biosynthesis) and aureobasidin A

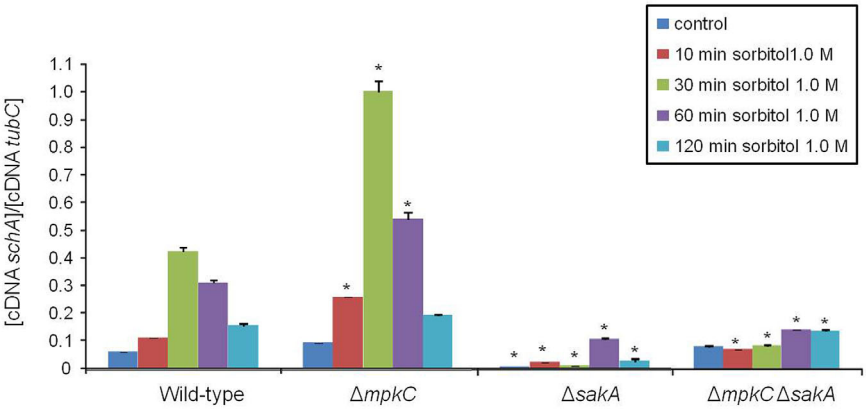

Fig. 4. The *schA* expression upon osmotic stress is dependent on SakA. The wild-type, Δ*sakA*, Δ*mpkC*and Δ*mpkC* Δ*sakA*mutants were grown for 18 h at 37°C. Then, sorbitol (1 M final concentration) was added for 0 (control), 10, 30, 60 and 120 min. The mycelium was harvested at the indicated times, and total RNA was extracted. The absolute quantitation of *schA* and *tubC* was determined by a standard curve (i.e., C_T –values plotted against a logarithm of the DNA copy number). The results are the means (± standard deviation) of four biological replicates (*, $p < 0.001$, comparison of the treatments with wild−type).

(an inhibitor of inositol phosphorylceramide (IPC) synthase) as the wild-type strain (Fig. 8B; data not shown). We also changed the balance in intermediary sphingolipid metabolites to disturb cell viability and growth by adding phytosphingosine (PHS) and dihydrosphingosine (DHS). PHS was able to inhibit Δ*schA* growth more than the wild-type and complementing strains, while all three strains showed the same degree of inhibition to DHS (Fig. 8A; data not shown). Sphingolipid profiling in the presence of osmotic stress (1 h Sorbitol 1.0 M) showed that the Δ*schA* mutant had reduced levels of hexosyl ceramides (HexCer), hydroxyceramides (OH-Cer), dihydroceramide species (dhCer), sphingosine (Sph), sphingosine 1-phosphate (Sph-1-P), ceramides (Cer), phytoceramide species with acyl chains of different length (αOHPhytoCer), phytoceramide species (PhytoCer) and inositol phosphorylceramide (IPC) (Fig. 8B; Table 1). In the absence of osmotic stress, Δ*schA* showed only reduced levels of dhCer, αOHPhytoCer and increased levels of MIPC (Fig. 8B and Table 1). Taken together, these results suggest that SchA influences sphingolipid biosynthesis primarily upon osmotic stress.

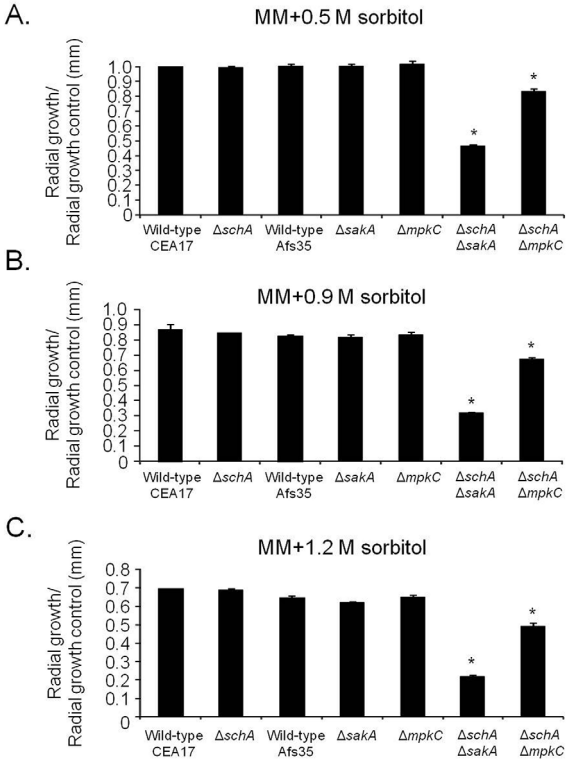

Fig. 5. The *A. fumigatus* Δ*schA* genetically interacts with Δ*sakA* and Δ*mpkC* upon osmotic stress. Wild-type (CEA17 pyrG$^+$ or AfS35), Δ*schA*, Δ*sakA*, Δ*schA* Δ*sakA*, Δ*mpkC*, Δ*schA* Δ*mpkC* were grown in MM with increasing concentrations of sorbitol for 72 h at 37°C. The data are expressed as radial growth sorbitol/radial growth control (mm). The radial diameter data are expressed as average ± standard deviation of three independent biological repetitions (* denotes $p < 0.001$, by *t*-tests when compared to the wild-type strain).

High-troughput data suggests a temporal program for osmotic stress response modulated by SchA

RNA-sequencing and proteomics were used to interrogate how the *A. fumigatus* wild-type and Δ*schA* strains adapt to long exposure to osmotic stress (1.0 M Sorbitol), with the objective of identifying possible SchA targets. We have used long exposure to osmotic stress because all our previous data suggest that SchA is important to modulate the strength of the signal since during its absence SakA remains longer time phosphorylated (see Fig. 3). The genes that were transcriptionally modulated post transfer to osmotic stress (1 h in 1.0 M Sorbitol) were identified (Supporting Information Fig. S1 and Tables S1 and S2), revealing 986 and 680 genes up or downregulated, respectively in the wild-type, and 1,152 and 799 genes up or downregulated in the Δ*schA* strain ($-1.0 \geq \log2FC \geq 1.0$). A comparison of the differentially expressed genes showed 324 genes which are either more highly expressed (151) or less expressed (173) in the Δ*schA* mutant in comparison to the wild-type strain (Supporting Information Tables S1 and S2).

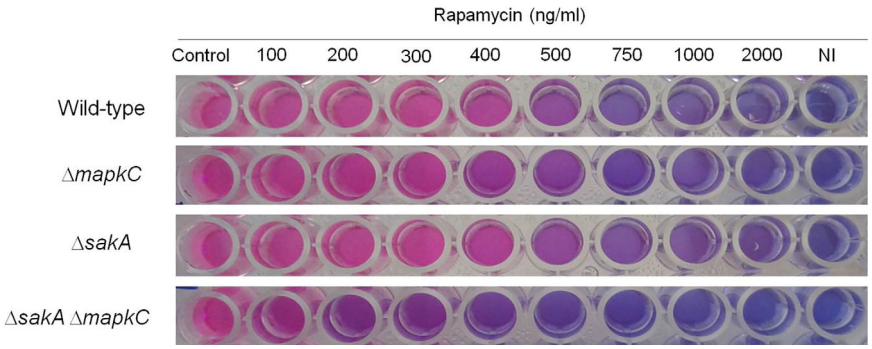

Fig. 6. The *A. fumigatus* Δ*mpkC* and Δ*mpkC* Δ*sakA* mutants are more sensitive to rapamycin. The strains were inoculated in YG medium + Alamar Blue with increasing concentrations of rapamycin, and incubated for 48 h at 37°C. This experiment was repeated three times and the experiment that is shown here is is a representative experiment.

Gene Ontology (GO) enrichment analyses of the differentially expressed genes in Δ*schA* showed a transcriptional downregulation of mitochondrial metabolism and function, ion transport, intracellular protein transmembrane and vacuolar transport, cofactor biosynthetic process, nucleotide biosynthetic process and cellular nitrogen compound biosynthetic process (Table 2). Conversely, there was an upregulation of genes encoding proteins involved in numerous biosynthetic processes, including hexose metabolic process, pentose-phosphate shunt and NADPH regeneration, alcohol metabolic process, DNA-dependent DNA replication and cell cycle, RNA metabolic process, ribosome biogenesis and translational initiation and monosaccharide catabolic process (Table 2). Therefore, this analysis of the transcriptome implies that upon prolonged osmotic stress SchA is important for mitochondrial function and intracellular transport, while its absence increases the expression of genes important for monosaccharide metabolism and cell cycle progression.

We also used label-free quantitative proteomics (spectral counts) to investigate proteins differentially abundant in the Δ*schA* mutant upon osmotic stress (Supporting Information Tables S3–S5, Tables 3 and 4). Proteins of significant differential abundance in Δ*schA* were classified in terms of biological function. Upon osmotic stress, in Δ*schA*, there was a reduction in abundance of proteins related to RNA and protein synthesis, chromatin modification, lipid metabolism and the glycerol-3-phosphate dehydrogenase (Table 3). Upon osmotic stress, in Δ*schA*, there was an increase in protein abundance related to oxidative and osmotic stresses (Table 4). Therefore, this proteomic analysis implies that upon prolonged osmotic stress the absence of SchA promotes oxidative stress response, phosphatidic acid synthesis and carbohydrate metabolism.

The integration of the transcriptomics, proteomics and large-scale lipid analysis strongly supports the notion that the SchA has an influence on the hyperosmotic stress response network in *A. fumigatus*. In fact, the analysis of all three independent approaches shows that while under normal growth condition only minor differences are noted between wild-type and *schA* mutant strain, a strong difference in the RNA, protein and lipid composition is noticed between both strains under osmotic stress. In the case of RNA expression, most of the initial differences noticed between both strains are augmented after 1 h exposition to osmotic stress. As shown in Fig. 9A (and Supporting Information Table S6), 36 genes are induced in the mutant strain while 73 are repressed (groups C2, C3 and C7), while 8 genes (group C1) are induced in the mutant strain at the initial condition but are not differentially expressed upon osmotic stress. Accordingly, groups C4 and C8 represent genes induced (116 genes) or repressed (100 genes) in the mutant strain upon osmotic stress that are not differentially expressed during normal growth conditions. Finally, five genes were found to be repressed in the mutant under normal growth but induced upon osmotic stress (group C5), while three genes repressed under normal growth were not differentially expressed upon 1 h exposure to the osmotic stress (group C6).

The analysis of the proteomics data allows the observation of a more complex behavior, since the effect of osmotic stress was quantified after 2 and 4 h. In fact, the proteomics analysis demonstrated again that under normal growth, only few proteins are differentially abundant in the mutant compared to the wild-type strain. However, upon exposition to osmotic stress, the number of proteins differentially abundant grows five-times, and several different profiles were observed. Most of these differences in the proteome occurs in the first 2 h of stress and disappears upon prolonged exposition, as indicated for 42 proteins with higher levels (group C1, Fig. 9B and Supporting Information Table S6) and 41 proteins with lower levels (group C6), indicating that in these cases the proteome returns to a steady-state condition. From these two groups, we found that a significant amount of the proteins from group C1 are related to *Protein Synthesis* (17 proteins) and *Osmotic and Oxidative Stress* (6 proteins), while group C6 is abundant

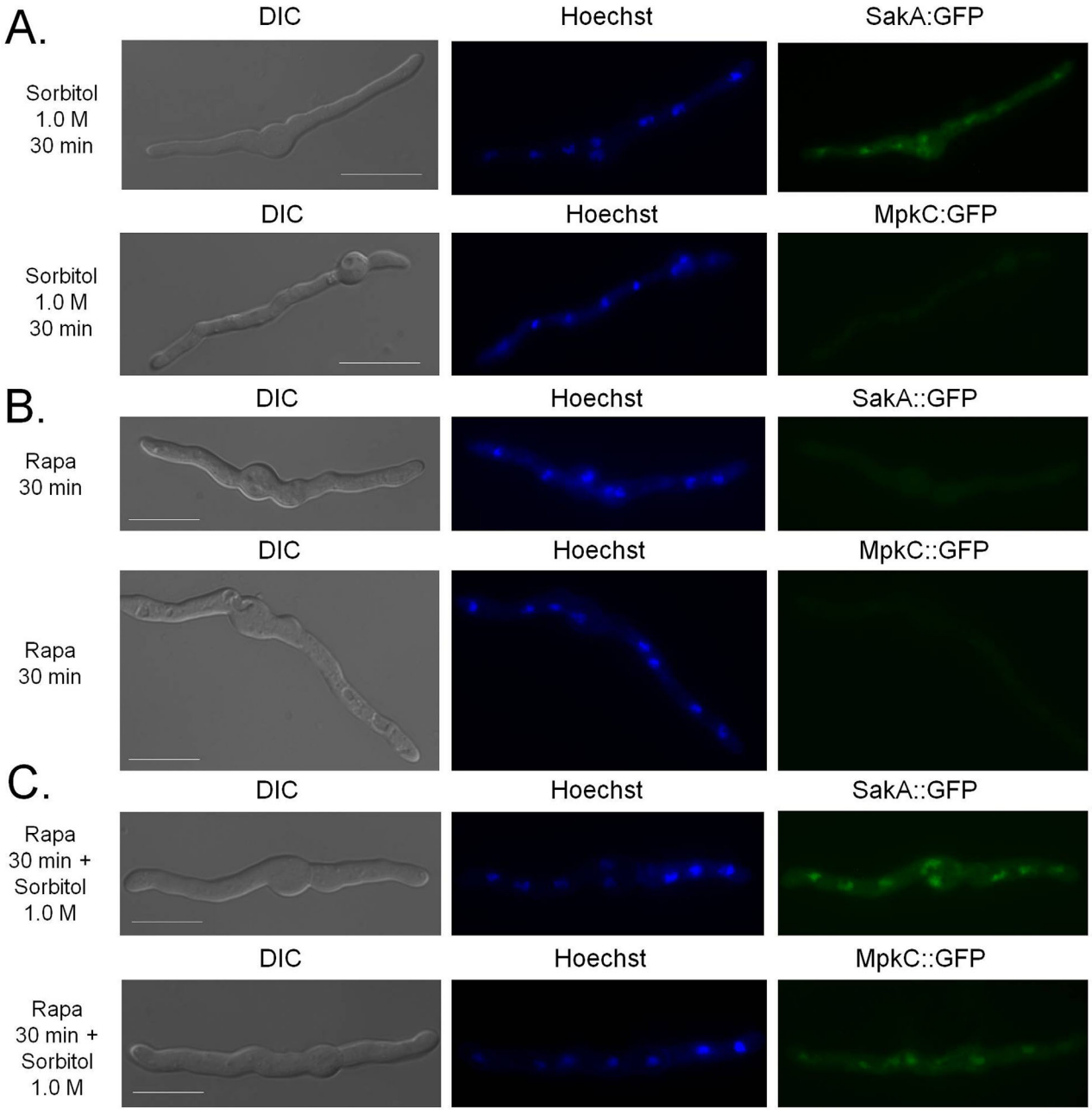

Fig. 7. MpkC::GFP migrates to the nucleus upon osmotic stress in the presence of rapamcyin.
A. The SakA::GFP and MpkC::GFP strains were grown for 16 h at 30°C in MM and incubated for 30 min in the presence of 1.0 M sorbitol at 30°C,
B. rapamycin 2 μg/ml for 30 min at 30°C or
C. rapamycin 2 μg/ml combined with 1.0 M sorbitol for 30 min at 30°C. Bars, 5 μm.

for genes also related to *Protein Synthesis* (14 proteins) and *Chromatin Modification* (7 proteins). A reduced but still significant number of proteins only appears after prolonged exposition to osmotic stress (4 h), with 28 proteins being highly abundant (group C5) and 10 proteins with reduced levels (C8). Quite interestingly, analysis of these late proteins reveals enrichment for *Osmotic and Oxidative Stress* proteins at group C5 (9 out of 28) and 3 proteins related to *Protein Synthesis* at group C8 (3 out of 10). It is quite remarkable as well that from the proteins differentially expressed in normal growth conditions but not signifcantlly upon osmotic stress (groups C4 and C10), 7 out of 10 genes with lower level in mutant stress are related to *Protein Synthesis* (group C10).

In other words, the comparison of early and late-induced proteins upon osmotic stress indicates that the

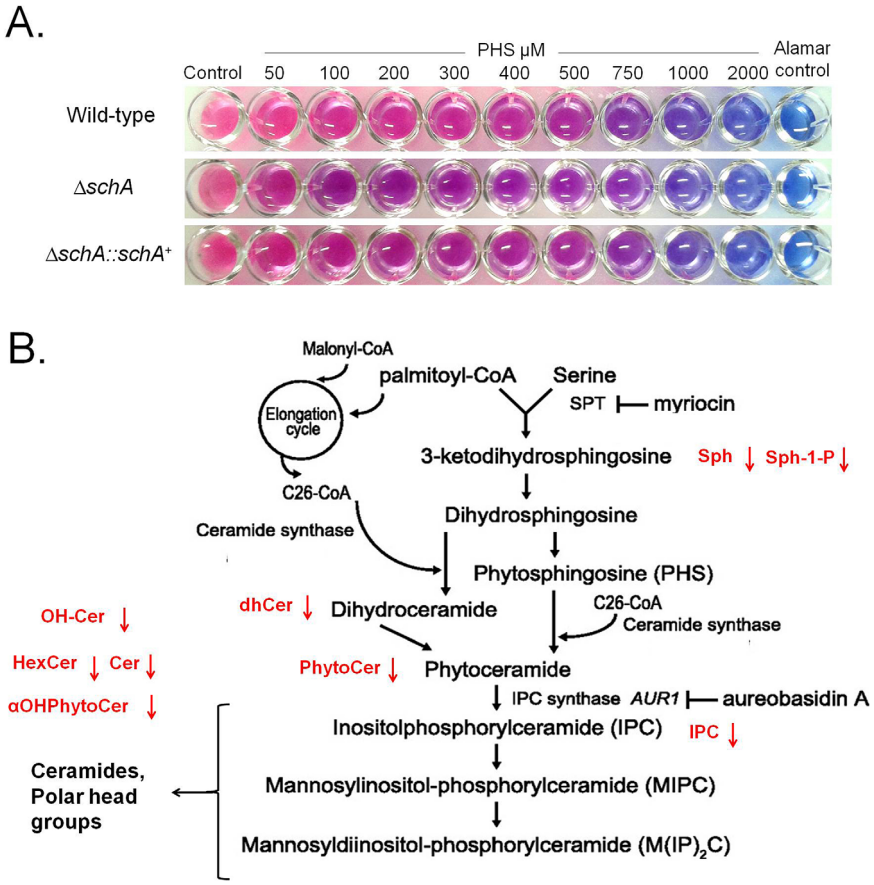

Fig. 8. The Δ*schA* mutant has reduced sphingolipids production.
A. The wild-type, Δ*schA*, and Δ*schA::schA*$^{+}$ strains were inoculated in MM medium + Alamar Blue with increasing concentrations of phytosphingosine (PHS), and incubated for 48 hrs at 37°C.
B. Schematic representation of the sphingolipids biosynthesis pathway (adapted from Swinnen *et al.*, 2014b) showing in red the reduction of different intermediaries or products. HexCer= hexosyl ceramides; OH-Cer= hydroxyceramides; dhCer= dihydroceramide species; Sph= sphingosine; Sph-1-P= sphingosine 1-phosphate; Cer= ceramides; αOHPhytoCer= phytoceramide species with acyl chains of different length; PhytoCer= phytoceramide species; and IPC= inositol phosphorylceramide.

first response is enriched for proteins related to 'Protein Synthesis' while encompass only a few proteins related to 'Oxidative and Osmotic Stress'. However, the late-induced group has no proteins related to 'Protein Synthesis' but a larger amount of proteins related to 'Oxidative and Osmotic Stress'. This analysis indicates the existence of a temporal program regulated by SchA in *A. fumigatus* that is activated when this fungus is

Table 1. Lipids distribution in the wild-type and Δ*schA* upon non-stress (control) and osmotic stress conditions (Sorbitol 1.0 M).

	Wild-type	Δ*schA*	Wild-type X Δ*schA*	Wild-type Sorbitol 1.0 M	Δ*schA*	Wild-type X Δ*schA*
Lipids[a]	**Control** ([b])	**Control**	(***p*-values**[c])		**Sorbitol 1.0 M**	**Sorbitol (*p*-values**[c])
HexCer	4.040 ± 0.363	3.610 ± 0.939	0.314	4.264 ± 0.219	1.043 ± 0.086	**0.000**
OH-Cer	0.124 ± 0.016	0.103 ± 0.020	0.178	0.142 ± 0.017	0.029 ± 0.005	**0.001**
dhSph	0.040 ± 0.002	0.044 ± 0.005	0.193	0.065 ± 0.032	0.023 ± 0.004	0.092
dhSph-1-P	0.001 ± 0.001	0.001 ± 0.000	0.277	0.000 ± 0.000	0.000 ± 0.000	0.445
dhCer	0.404 ± 0.023	0.316 ± 0.019	**0.011**	0.216 ± 0.004	0.113 ± 0.008	**0.000**
Sph	0.059 ± 0.013	0.073 ± 0.025	0.280	0.030 ± 0.006	0.031 ± 0.008	0.431
Sph-1-P	0.000 ± 0.000	0.001 ± 0.000	0.071	0.000 ± 0.000	0.000 ± 0.000	**0.032**
Cer	0.632 ± 0.103	0.466 ± 0.061	0.082	0.464 ± 0.084	0.154 ± 0.020	**0.006**
αOHPhytoCer	0.353 ± 0.004	0.257 ± 0.011	**0.000**	0.224 ± 0.079	0.063 ± 0.007	**0.034**
PhytoCer	2.414 ± 0.660	2.028 ± 0.101	0.259	1.623 ± 0.220	0.392 ± 0.057	**0.001**
IPC	0.495 ± 0.042	0.518 ± 0.238	0.457	0.626 ± 0.173	0.106 ± 0.010	**0.011**
MIPC	0.012 ± 0.003	0.023 ± 0.002	**0.010**	0.005 ± 0.002	0.005 ± 0.002	0.474

[a]**HexCer**= hexosyl ceramides; **OH-Cer**= hydroxyceramides; **dhSph**= dihydrosphingosine; **dhSph-1-P**= dihydrosphingosine 1-phosphate; **dhCer**= dihydroceramide species; **Sph**= sphingosine; **Sph-1-P**= sphingosine 1-phosphate; **Cer**= ceramides; **αOHPhytoCer**= phytoceramide species with acyl chains of different length; **PhytoCer**= phytoceramide species; **IPC**= inositol phosphorylceramide; and **MIPC**= mannosylinositol phosphorylceramide
[b]Data represented as pmol/Pi (Mean of three repetitions ± SEM).
[c]Student's *t*-test.

Table 2. A summary of the GO terms over-represented up or down regulated in log2FC Δ*schA* versus wild-type post transfer to 1 M Sorbitol for 1 h. For the full list refer to Supporting Information Table S1. BP = Biological Process.

GO term	Description	*p*-value	Class	Reg
GO:0042375	Quinone cofactor metabolic process	0,000186	BP	Down
GO:0045324	Late endosome to vacuole transport	0,002303	BP	Down
GO:0006626	Protein targeting to mitochondrion	3,08E-07	BP	Down
GO:0034220	Ion transmembrane transport	0,000309	BP	Down
GO:0051188	Cofactor biosynthetic process	0,001837	BP	Down
GO:0009165	Nucleotide biosynthetic process	0,001054	BP	Down
GO:0015992	Proton transport	6,37E-08	BP	Down
GO:0072655	Establishment of protein localization in mitochondrion	1,59E-07	BP	Down
GO:0044271	Cellular nitrogen compound biosynthetic process	0,002281	BP	Down
GO:0006623	Protein targeting to vacuole	0,001624	BP	Down
GO:0007006	Mitochondrial membrane organization	3,18E-05	BP	Down
GO:0006839	Mitochondrial transport	9,48E-07	BP	Down
GO:0006091	Generation of precursor metabolites and energy	6,44E-06	BP	Down
GO:0007034	Vacuolar transport	0,00019	BP	Down
GO:0061024	Membrane organization	0,000836	BP	Down
GO:0000002	Mitochondrial genome maintenance	0,001626	BP	Down
GO:0071806	Protein transmembrane transport	0,002165	BP	Down
GO:0065002	Intracellular protein transmembrane transport	0,002165	BP	Down
GO:0007007	Inner mitochondrial membrane organization	0,000442	BP	Down
GO:0006123	Mitochondrial electron transport, cytochrome c to oxygen	0,000622	BP	Down
GO:0006886	Intracellular protein transport	0,000151	BP	Down
GO:0030150	Protein import into mitochondrial matrix	0,000856	BP	Down
GO:0006139	Nucleic acid metabolic process	5,91E-16	BP	Up
GO:0046365	Monosaccharide catabolic process	1,06E-05	BP	Up
GO:0007049	Cell cycle	0,001353	BP	Up
GO:0016070	RNA metabolic process	4,06E-15	BP	Up
GO:0006298	Mismatch repair	0,002667	BP	Up
GO:0006740	NADPH regeneration	0,00093	BP	Up
GO:0042254	Ribosome biogenesis	2,93E-34	BP	Up
GO:0006413	Translational initiation	0,001423	BP	Up
GO:0006007	Glucose catabolic process	0,001423	BP	Up
GO:0019320	Hexose catabolic process	0,000514	BP	Up
GO:0006261	DNA-dependent DNA replication	2,11E-05	BP	Up
GO:0006066	Alcohol metabolic process	0,002778	BP	Up
GO:0019318	Hexose metabolic process	0,002044	BP	Up
GO:0006098	Pentose-phosphate shunt	0,002457	BP	Up
GO:0034471	ncRNA 5'-end processing	6,56E-09	BP	Up
GO:0031126	snoRNA 3'-end processing	0,002457	BP	Up
GO:0006807	Nitrogen compound metabolic process	2,93E-13	BP	up

exposed to osmotic stress conditions. To the best of our knowledge, this is the first time such comprehensive high-throughput analysis is used to investigate the functional scope of a Sch9 homologue.

SchA is involved in sensing iron availability

Recently, Baldin *et al*. (2015) demonstrated that in *A. fumigatus* the repression of TOR disrupted iron regulation. We investigated the response of Δ*schA* to iron starvation or excess. *A. fumigatus* cannot directly use human iron sources such as heme, ferritin or transferrin (Schrettl and Haas, 2011; Moore, 2013). It utilizes both reductive iron assimilation (RIA) and siderophore (low-molecular-mass ferric iron chelators)-mediated iron uptake during murine infection (Schrettl and Haas, 2011; Moore, 2013). Two master transcription factors regulate iron assimilation, HapX (during starvation but also can affect iron excess) and SreA (during iron repletion or excess) (Schrettl and Haas, 2011; Moore, 2013; Gsaller *et al*., 2014). There was no difference in growth between strains in MM or iron excess. However, the Δ*schA* mutant grew approximately 20% more than the wild-type and the complemented strains during iron starvation (Fig. 10A and data not shown). Western blot analysis showed that both iron starvation and excess decrease total Rps6 (Fig. 10A). Iron excess increases the ratio of Rps6-P/Rps6 in the wild-type (40 and 60% in 1 and 2 h iron excess) and in the Δ*schA* mutant is about the same and 48% lower than the control (in 1 and 2 h iron starvation) (Fig. 10B). During iron starvation the ratio of Rps6-P/Rps6 increases 1.9-fold and 2.3-fold in the wild-type than in the control while in the Δ*schA* there is 70% less and 30% more Rps6-P/Rps6 than in the control (Fig. 10B).

The wild-type, Δ*hapX*, and Δ*sreA* mutants were grown for 24 h in iron replete or iron starvation conditions and then exposed to either iron starvation or iron excess for 1 or 2 h (Fig. 10C). During iron starvation, the wild-type strain exhibited increased *schA* expression, while in the Δ*hapX* and Δ*sreA* mutants *schA* showed constant levels of expression (Fig. 10C, left panel). During iron excess, the wild-type, Δ*hapX*, and Δ*sreA* strains showed similar levels of *schA* expression (Fig. 10C, right panel). As expected the wild-type strain showed increased *hapX* and *sidA* (L-ornithine N^5-oxygenase; the first committed step in siderophore biosynthesis) expression during iron starvation, while the transcriptional response was higher in the Δ*schA* mutant (Fig. 10D). During iron excess, *hapX* and *sidA* expression was slightly decreased in the wild-type strain, while in the Δ*schA* mutant, *hapX* has about the same expression levels while *sidA* has slightly decreased levels than the wild-type (Fig. 10D). Surprisingly, in the wild-type strain there is an unexpected low induction of the *sreA* gene during iron starvation conditions while this was not observed in the Δ*schA* mutant (Fig. 10D).

To have a preliminary insight of the compounds which are accumulating during iron starvation or excess, we grew the wild-type and Δ*schA* strains for 48 h in liquid MM with iron starvation or 200 μM $FeSO_4$, and extracted the intracellular polar compounds for gas chromatography coupled to mass-spectrometry (GC-MS) analysis. Principal Component Analyses (PCA) demonstrated that the first source of variation in their metabolome, the amino acids and some other primary metabolites of the wild-type and Δ*schA* strains, were distinct under the different conditions (Supporting Information Table S7; Fig. 10E and F). Tables 5 and 6 show the values of fold increase during iron starvation or excess versus the control, comparing the Δ*schA* and wild-type strains. During iron starvation, most of the amino acids in both strains dramatically decreased when compared to the control (Table 5). However, this decrease was greater in the Δ*schA* mutant. Interestingly, there was a much higher accumulation of ornithine, pyruvate, succinate and trehalose in the Δ*schA* mutant compared to the wild-type strain. In contrast, isocitrate and malate showed a moderately higher level of accumulation in the Δ*schA* mutant when compared to the wild-type strain. Upon iron excess, a less dramatic alteration was observed. Nonetheless there was an increased utilization of malate and increased accumulation of trehalose in the Δ*schA* mutant when compared to the wild-type strain (Table 6). Therefore, SchA appeared to influence both ornithine and general amino acid biosynthesis and metabolites in the glyoxylate pathway, in addition to trehalose biosynthesis.

SchA is important for A. fumigatus virulence in a low dose murine infection

We have used a neutropenic murine model of invasive pulmonary aspergillosis to evaluate *A. fumigatus* Δ*schA* pathogenicity (Fig. 11A). The infection by the wild-type strain resulted 100% mortality after 13 days post-infection; however, Δ*schA* infection yielded a significantly reduced mortality rate of about 20% after 15 days post-infection (Fig. 11A, $p < 0.001$ and $p < 0.0038$ for the comparison between the wild-type strain and the Δ*schA* mutant, Log−rank, Mantel−Cox and Gehan−Breslow−Wilcoxon tests respectively). We have restored the virulence in an independent strain produced from a single ectopic reintegration of the wild-type *schA* locus. No statistical difference was observed between the wild-type and the complemented Δ*schA::schA*$^+$ strains (Fig. 11A, $p > 0.90$ and $p > 0.82$ for the comparison between the wild-type and the complemented strains, Log−rank, Mantel−Cox and Gehan−Breslow−Wilcoxon tests respectively), directly linking the attenuation of Δ*schA* virulence to SchA function.

Histopathological examination revealed that at 72 h post-infection the lungs of mice infected with the wild-type strain contained multiple foci of invasive hyphal growth, which penetrated the pulmonary epithelium in major airways, while pockets of branched invading hypha originated from the alveoli (Fig. 11B). In contrast, Δ*schA* infections revealed inflammatory infiltrates in bronchioles, with some containing poorly germinated or ungerminated conidia (Fig. 11B). Fungal burden was measured by qPCR, showing that the Δ*schA* strain did not grow within the lungs as well as the wild-type and the complemented Δ*schA::schA*$^+$ strains (Fig. 11C, $p < 0.0001$ for the comparison between the wild-type and the Δ*schA* mutant, and $p > 0.05$ between the wild-type and the complemented strains). Taken together, this strongly indicates that SchA plays an important role in *A. fumigatus* virulence.

Discussion

We have characterized the *A. fumigatus* Sch9 homologue, SchA, as a substrate of TOR, which regulates diverse aspects of cell growth in response to intracellular and extracellular signals. In *S. cerevisiae* Sch9p plays multiple roles in stress resistance, longevity, sphingolipid biosynthesis and nutrient sensing (Smets *et al.*, 2010; Longo and Fabrizio, 2012; Spincemaille *et al.*, 2014; Swinnen *et al.*, 2014a, 2014b). Three of the six amino acid residues on the C-terminus of Sch9 which are phosphorylated by TORC1 were conserved in SchA. We previously identified SchA as a target for the calcineurin-

Table 3. Proteins identified as less expressed in the Δ*schA* mutant strain upon growth on YPD medium (time 0 h) and transfer to 1.0 M Sorbitol (for 2 or 4 h). For the full list refer to Supporting Information Tables S3–S5.

Aspergillus fumigatus			Δ*schA* x Wild type (t-test difference)		
Strain Af293	**Strain A1163**	**Protein annotation**	**0 h**	**2 h**	**4h**
RNA and Protein synthesis					
AFUA_7G04280	AFUB_089820	Small nuclear ribonucleoprotein (LSM5)	NI[a]	NI	−2.1380
AFUA_1G04280	AFUB_004610	30S ribosomal protein S7	−1.0016	NI	NI
AFUA_1G06770	AFUB_007150	40S ribosomal protein S26	−1.2207	NI	NI
AFUA_1G14220	AFUB_013760	nopA. Nucleolar protein	NI	−1.29947	NI
AFUA_2G07970	AFUB_023990	60S ribosomal protein	−1.6866	NI	NI
AFUA_3G13480	AFUB_035720	Translation initiation factor 2 alpha subunit	NI	−1.36763	NI
AFUA_3G13400	AFUB_035810	nop5. Putative nucleolar protein	NI	−3.09814	NI
AFUA_3G13310	AFUB_035890	Ribosomal protein S15. Putative	NI	NI	−1.0561
AFUA_3G10800	AFUB_038330	Eukaryotic translation initiation factor 3 subunit CLU1/TIF31	NI	−2.73375	−1.6641
AFUA_3G09600	AFUB_039570	sik1. Ortholog(s) have role in rRNA processing and 90S preribosome.	NI	−5.59322	NI
AFUA_3G08600	AFUB_040500	Translational initiation factor 2 beta	NI	−1.65107	NI
AFUA_3G06840	AFUB_042210	40S ribosomal protein S4	−1.286	NI	NI
AFUA_6G03580	AFUB_094710	mRNA-nucleus export ATPase (Elf1)	−1.0381	NI	NI
AFUA_6G02520	AFUB_095820	Eukaryotic translation initiation factor eIF-1A subunit	NI	−1.37648	NI
AFUA_6G02440	AFUB_095900	60S ribosomal protein L24a	−1.2355	NI	NI
AFUA_7G05290	AFUB_090870	40S ribosomal protein	−1.3228	NI	NI
AFUA_1G05310	AFUB_005660	nucleolus localization	NI	−1.83611	NI
AFUA_8G02730	AFUB_083860	Translation machinery-associated protein 22	NI	−1.00583	NI
AFUA_4G10550	AFUB_067650	small nucleolar ribonucleoprotein complex component (Utp5)	NI	−1.39821	NI
AFUA_1G03970	AFUB_004370	Putative mitochondrial translation initiation factor IF-2	NI	−1.03423	−1.24289
AFUA_5G11000	AFUB_058570	U2 small nuclear ribonucleoprotein A' (U2 snRNP-A')	NI	−1.18664	NI
AFUA_5G03470	AFUB_051980	tRNA-guanine transglycosylase family protein	−1.4233	NI	−1.90945
AFUA_1G05560	AFUB_005900	Ortholog(s) have role in cytoplasmic translation	NI	−1.56902	NI
AFUA_3G06010	AFUB_043040	RNA processing protein Emg1. Putative	NI	−1.0297	NI
AFUA_6G05080	AFUB_093200	CCR4 Associated Factor	NI	NI	−1.10484
AFUA_2G05950	AFUB_022990	RNA binding activity and role in mRNA splicing. via spliceosome	NI	−1.42661	NI
AFUA_4G07580	AFUB_064670	translation initiation factor EF-2 gamma subunit	NI	−1.90111	NI
Chromatin modification					
AFUA_1G09600	AFUB_009050	Putative GNAT-type acetyltransferase	NI	−2.2675	NI
AFUA_1G13780	AFUB_013260	Histone H4.1. core histone protein; nearly identical to histone H4.	NI	−1.05959	NI
AFUA_2G03390	AFUB_020460	rpdA. putative histone deacetylase	NI	−1.07917	NI
AFUA_3G06070	AFUB_042980	histone H1	NI	−2.60937	NI
AFUA_3G05360	AFUB_043640	histone H2A	NI	−1.60511	NI
AFUA_3G05350	AFUB_043650	Histone H2B	NI	−1.49352	NI
AFUA_4G11910	AFUB_068910	N-terminal acetyltransferase catalytic subunit (NAT1)	NI	−2.76482	NI
Lipid metabolism					
AFUA_7G05920	AFUB_091500	stearic acid desaturase (SdeA)	NI	−1.04105	NI
AFUA_7G03740	AFUB_089270	14-alpha sterol demethylase14-alpha sterol demethylase Cyp51B	NI	−1.04625	NI
Miscellaneous					
AFUA_1G05320	AFUB_005670	role in cell redox homeostasis. glycerol ether metabolic process	NI	−1.26321	NI
AFUA_6G13420	AFUB_001330	Ubiquitin-like protein DskB. Putative	NI	NI	−1.25449
AFUA_1G08810	AFUB_008170	Glycerol-3-phosphate dehydrogenase	−2.6886	NI	−1.23237
AFUA_1G10380	AFUB_009800	Non-ribosomal peptide synthetase (NRPS);essential for fumigaclavine C	NI	−1.70174	−1.27983
AFUA_1G10400	AFUB_009820	Putative nuclear pore complex protein	NI	−1.04484	NI
AFUA_4G04740	AFUB_098260	Ran guanyl-nucleotide exchange factor activity. signal transducer activity	NI	−1.39637	NI

Table 3: *Continued*

Aspergillus fumigatus			ΔschA x Wild type (t-test difference)		
Strain Af293	**Strain A1163**	**Protein annotation**	**0 h**	**2 h**	**4h**
AFUA_2G11020	AFUB_026790	Putative triose-phosphate isomerase	−1.3098	NI	NI
AFUA_3G05580	AFUB_043410	Chitin synthase activator (Chs3)	NI	NI	−1.18957
AFUA_5G01940	AFUB_050460	R3H domain protein. putative. ssRNA binding protein	NI	−1.35519	NI
AFUB_051760	AFUB_051760	ubiquitin C-terminal hydrolase (HAUSP)	NI	−1.00107	NI
AFUB_052020	AFUB_052020	alpha glucosidase II. alpha subunit	NI	−1.27163	NI
AFUA_5G09910	AFUB_057500	Nitroreductase family protein. Putative	−1.2944	NI	NI
AFUA_5G11760	AFUB_059330	Hydroxymethylbilane synthase. Putative	NI	NI	−1.12319
AFUA_4G07160	AFUB_064250	ATP dependent RNA helicase (Dob1)	NI	−1.50385	NI
AFUA_4G07660	AFUB_064750	secretory component protein shr3	NI	−1.18606	NI
AFUA_4G08710	AFUB_065800	short chain dehydrogenase	−1.4619	NI	NI
AFUA_4G08710	AFUB_065800	Putative short chain dehydrogenase	NI	NI	−1.33766
AFUA_4G09660	AFUB_066770	secretory component protein shr3	NI	−1.15888	NI
AFUA_6G06620	AFUB_072550	COPII vesicles protein Yip3	NI	NI	−1.43633
AFUA_6G07210	AFUB_073150	Sod4. Putative copper-zinc superoxide dismutase (1)	NI	NI	−1.58874
AFUA_6G08580	AFUB_074540	FKBP-type peptidyl-prolyl isomerase	NI	−3.77503	NI
AFUA_7G01220	AFUB_087800	Farnesyl-diphosphate farnesyltransferase	NI	−1.01045	NI
AFUA_7G02230	AFUB_088780	mRNA binding post-transcriptional regulator (Csx1)	NI	−1.62588	NI
Unknown					
AFUA_1G04550	AFUB_004890	Uncharacterized	NI	−1.41957	NI
AFUA_2G02630	AFUB_019730	Protein of unknown function	NI	NI	−4.09779
AFUA_1G06780	AFUB_007160	Ortholog(s) have cytosol. nucleus localization	NI	−1.16415	NI
AFUA_2G05670	AFUB_022700	Protein of unknown function	NI	−1.05243	NI
AFUA_2G12580	AFUB_028240	Ortholog(s) have endoplasmic reticulum localization	NI	−1.40812	NI
AFUA_3G07710	AFUB_041390	Has domain(s) with predicted nucleic acid binding. nucleotide binding activity	NI	−2.62475	NI
AFUA_8G04570	AFUB_082920	PWWP domain protein	NI	−1.71027	NI

[a]NI = not identified, the protein was not identified in this timepoint.

CrzA pathway in response to calcium stress, while also demonstrating that the genetic interaction between the calcineurin-CrzA and HOG pathways was essential for full virulence (de Castro *et al*., 2014). Several members of the two-component system (TCS) and the HOG pathway were more sensitive to calcium (de Castro *et al*., 2014). Interestingly, the Δ*schA* mutant was more sensitive to calcium, rapamycin and osmotic stress, suggesting its involvement in all three signaling pathways.

The highly conserved MAPK signaling pathways are essential for the adaptation to environmental changes (Pearson *et al*., 2001; Rispail *et al*., 2009). The MAPK cascades are important for relaying, integrating and amplifying intracellular signals, and are crucial signaling components involved in many cellular processes (Pearson *et al*., 2001; Rispail *et al*., 2009). In *A. fumigatus* MpkC and SakA are paralogues of the *S. cerevisiae* Hog1, which is the main regulator of the HOG pathway (Maeda *et al*., 1994). SakA and MpkC play a role in carbon utilization and adaptations to the antifungal agent, caspofungin (Reyes *et al*., 2006; Altwasser *et al*., 2015; Valiante *et al*., 2015). Pascual-Ahuir and Proft (2007) have shown that Sch9 is involved in the regulation of adaptations to acute hyperosmotic stress in *S. cerevisiae*. Here, we demonstrated that the expression of *schA* was dependent on SakA, while SchA modulated SakA phosphorylation and increased expression and protein accumulation of several downstream targets by transcriptomics and proteomics. Accordingly, the double mutants Δ*schA* Δ*sakA* and Δ*schA* Δ*mpkC* were more sensitive to osmotic stress, suggesting these pathways genetically interacted upon osmotic stress. Additional evidences for an interaction between TOR and SakA/MpkC MAP kinases are: (i) increased rapamycin sensitivity of Δ*sakA* Δ*mpkC*, and (ii) upon osmotic stress, SakA::GFP was translocated to the nucleus quicker than MpkC::GFP, while rapamycin accelerated the translocation of MpkC::GFP to the nucleus during osmotic stress. These results suggest that MpkC could act by modulating SakA activity upon exposure to osmotic stress and this was controlled by the TOR pathway. Recently, in *F. graminearum* FgSch9 and FgHog1 null mutants exhibited increased sensitivity to osmotic and oxidative stresses, and this defect was more severe in

Table 4. .Proteins identified as more expressed in the ΔschA mutant strain upon growth on YPD medium (time 0 h) and transfer to 1.0 M Sorbitol (for 2 or 4 h). For the full list refer to Supplementary Tables S3–S5.

Aspergillus fumigatus		Δ*schA* x Wild type(t-test difference)			
Strain Af293	**Strain A1163**	**Protein annotation**	**0 h**	**2 h**	**4 h**
oxidative and osmotic stresses					
AFUA_3G02270	AFUB_046060	mycelial catalase Cat1	1.505	NI[a]	NI
AFUA_6G12450	AFUB_078460	awh11. Putative heat shock protein	NI	NI	2.200
AFUA_3G14540	AFUB_034690	heat shock protein Hsp30/Hsp42	NI	1.068	NI
AFUA_6G12180	AFUB_078180	DprB. Fungal dehydrin-like protein	NI	6.192	1.394
AFUA_7G04520	AFUB_090060	DprC. Dehydrin-like protein	NI	NI	1.149
AFUA_7G02070	AFUB_088630	AIF-like mitochondrial oxidoreductase; conidia-enriched protein	NI	4.063	1.332
AFUA_8G01090	AFUB_085510	Putative thioredoxin; hypoxia repressed protein	NI	NI	1.459
AFUA_1G09890	AFUB_009330	Protein with Yap1-dependent induction in response to hydrogen peroxide	NI	1.341	NI
AFUA_4G14380	AFUB_071650	Glutathione S-transferase. Putative	NI	NI	1.176
AFUA_2G05060	AFUB_022090	Alternative oxidase. mediates the cyanide-insensitive respiratory pathway	NI	1.290	NI
AFUA_5G07000	AFUB_054560	Putative NAD binding Rossmann fold oxidoreductase	NI	NI	1.625
AFUA_1G02090	AFUB_002470	predicted oxidoreductase activity	NI	1.413	NI
AFUA_3G00330	AFUB_048120	NAD dependent epimerase/dehydratase family protein	NI	NI	1.911
AFUA_5G09910	AFUB_057500	nitroreductase family protein	NI	2.686	NI
AFUA_4G09220	AFUB_066340	flavin-binding monooxygenase-like protein	NI	NI	1.128
AFUA_8G04340	AFUB_083200	Cystathionine gamma-lyase	NI	1.160	NI
AFUA_8G06080	AFUB_081400	Putative flavohemoprotein	NI	NI	1.633
AFUA_1G09930	AFUB_009370	glycerol dehydrogenase; protein level decreases upon heat shock	NI	NI	1.040
Protein synthesis					
AFUA_5G05450	AFUB_053010	40S ribosomal protein S3Ae; 40S ribosomal protein S1	NI	1.953	NI
AFUA_4G07845	AFUB_064950	Ortholog(s) have cytosolic large ribosomal subunit	NI	2.226	NI
AFUA_6G02440	AFUB_095900	60s ribosomal protein L24	NI	1.354	NI
AFUA_7G05290	AFUB_090870	Cytosolic small ribosomal subunit S13/S15	NI	1.813	NI
AFUA_6G12720	AFUB_078720	40S ribosomal protein S29	NI	1.191	NI
AFUA_3G06840	AFUB_042210	Putative cytosolic small ribosomal subunit S4	NI	1.102	NI
AFUA_2G10300	AFUB_026110	40S ribosomal protein S17	NI	1.541	NI
AFUA_2G07970	AFUB_023990	60S ribosomal protein L19	NI	1.618	NI
AFUA_2G08130	AFUB_024140	Ortholog(s) have cytosolic large ribosomal subunit localization	NI	1.829	NI
AFUA_1G17120	AFUB_016510	Elongation factor 1 gamma	NI	2.034	NI
AFUA_3G06640	AFUB_042410	40S ribosomal protein S27	NI	1.688	NI
AFUA_2G03380	AFUB_020450	Ortholog(s) have cytosolic large ribosomal subunit	NI	2.383	NI
AFUA_1G06770	AFUB_007150	40S ribosomal protein S26	NI	1.851	NI
AFUA_2G11850	AFUB_027590	Allergenic ribosomal L3 protein	NI	1.510	NI
AFUA_1G09440	AFUB_008890	40S ribosomal protein S23	NI	2.711	NI
AFUA_1G16523	AFUA_1g16523	cytosolic small ribosomal subunit localization	NI	1.201	NI
AFUA_2G10440	AFUB_026240	Ortholog(s) have mRNA binding. small ribosomal subunit rRNA binding	NI	1.975	NI
Chromosome metabolism					
AFUA_2G14080	AFUB_029700	chromosome segregation protein SudA	NI	NI	1.435
AFUA_2G16080	AFUB_031760	role in mitotic sister chromatid cohesion and mating-type region	2.503	NI	NI
AFUA_3G14260	AFUB_034970	mismatched base pair and cruciform DNA recognition protein	NI	3.679	NI
AFUA_3G10480	AFUB_038680	meiotic sister chromatid recombination protein Ish1/Msc1	NI	1.129	NI
Phosphatidic acid metabolism					
AFUA_3G12330	AFUB_036830	Putative phosphatidyl synthase	NI	NI	1.896
AFUA_7G05580	AFUB_091160	Putative phospholipase D. pldA	NI	1.270	NI
AFUA_4G12000	AFUB_068990	phosphatidylinositol phospholipase C	1.089	NI	NI
AFUA_4G11720	AFUB_068730	Putative phosphatidyl synthase	NI	1.452	NI
Carbohydrate metabolism					
AFUA_2G15430	AFUB_031090	Sorbitol/xylulose reductase	NI	1.566	NI
AFUA_6G07720	AFUB_073680	Phosphoenolpyruvate carboxykinase AcuF.	1.233	NI	NI
AFUA_6G03540	AFUB_094750	Malate synthase AcuE	NI	NI	1.156

Table 4: *Continued*

Aspergillus fumigatus		ΔschA x Wild type(t-test difference)			
Strain Af293	**Strain A1163**	**Protein annotation**	**0 h**	**2 h**	**4 h**
Miscellaneous					
AFUA_2G04610	AFUB_021660	Role in post translational protein targeting to membrane and TRC complex	1.204	NI	1.543
AFUA_2G08920	AFUB_024830	GDSL Lipase/Acylhydrolase family protein	NI	NI	1.066
AFUA_2G08920	AFUB_031880	Uracil phosphoribosyltransferase	NI	NI	1.008
Afu2G16530	AFUB_032210	Cyanate hydratase	1.041	NI	NI
AFUA_3G07410	AFUB_041670	Putative isoamyl alcohol oxidase	NI	NI	1.138
AFUA_3G06660	AFUB_042390	Putaive NIPSNAP family protein	NI	NI	1.528
AFUA_3G00650	AFUB_047780	Lap2. Putative aminopeptidase Y	NI	NI	1.508
AFUA_5G02330	AFUB_050860	Major allergen and cytotoxin AspF1	NI	NI	1.168
AFUA_5G12590	AFUB_060250	Solid-state culture expressed protein (Aos23)	NI	NI	1.365
AFUA_4G05900	AFUB_062990	Transcript up-regulated in conidia exposed to neutrophils (2)	NI	NI	1.298
AFUA_4G08240	AFUB_065340	Putative zinc-containing alcohol dehydrogenase; conidia-enriched protein	NI	1.185	NI
AFUA_6G07590	AFUB_073550	Has domain(s) with predicted zinc ion binding activity	NI	1.634	NI
AFUA_6G07880	AFUB_073860	DUF500 and SH3 domain protein	1.072	NI	NI
AFUA_6G08750	AFUB_074710	PrncI, role in hyphal growth and cytosol. mitochondrion localization	NI	NI	1.313
AFUA_6G11430	AFUB_077440	AldA. Putative aldehyde dehydrogenase	1.003	NI	1.068
AFUA_8G05580	AFUB_081980	Putative coenzyme A transferase, coaT	NI	1.728	NI
AFUA_8G01930	AFUB_084680	Methyltransferase LaeA-like	1.183	NI	1.020
AFUA_8G00550	AFUB_086020	Putative methyl transferase; member of the pseurotin A gene cluster	2.742	NI	NI
AFUA_7G01000	AFUB_087580	Putative alcohol dehydrogenase involved in ethanol metabolism	1.659	NI	NI
AFUA_7G01340	AFUB_087920	Putative RPEL repeat protein	NI	NI	1.315
AFUA_7G06050	AFUB_091630	Ortholog(s) have SNARE binding. polyubiquitin binding activity	NI	1.158	NI
AFUA_6G04920	AFUB_093370	Putative NAD-dependent formate dehydrogenase, fdh	NI	2.031	NI
AFUA_4G04318	AFUB_098700	Copper resistance protein Crd2. similar to Cu-binding metallothionein	NI	2.265	NI
AFUA_3G07150	AFUB_041900	Succinate-semialdehyde dehydrogenase	1.141	NI	NI
AFUA_6G13330	AFUB_001440	Putative RNA binding protein of unknown function	NI	1.150	NI
Unknown					
AFUA_1G06350	AFUB_006730	Uncharacterized	NI	NI	1.301
AFUA_3G05610	AFUB_043380	Uncharacterized	NI	NI	1.020
AFUA_6G02535	AFUB_095800	Uncharacterized	NI	1.861	1.498
AFUA_4G02840	AFUB_100280	Uncharacterized	NI	3.513	NI
AFUA_3G02430	AFUA_3g02430	Uncharacterized	NI	NI	2.177
AFUA_8G05650	AFUB_081900	Hypothetical protein	NI	NI	1.784
AFUA_5G14890	AFUB_079000	Hypothetical protein	1.683	NI	1.298
AFUA_6G11850	AFUB_077850	Protein of unknown function; hypoxia induced protein	NI	1.908	NI
AFUA_5G13100	AFUB_060810	Hypothetical protein	NI	3.732	NI
AFUA_3G09990	AFUB_039180	Hypothetical protein	NI	1.452	NI
AFUA_1G13550	AFUB_013040	Uncharacterized	NI	3.024	NI
AFUA_1G15260	AFUB_014810	Uncharacterized	NI	NI	1.785
AFUA_1G08960	AFUB_008380	Uncharacterized	NI	NI	1.242

a. NI = not identified, the protein was not identified in this timepoint.

the FgSch9/FgHog1 double mutant (Gu *et al*., 2015). Glycerol and trehalose accumulation are conserved eukaryotic responses to hyperosmotic stress (Saito and Posas, 2012). Upon hypertonic stress, *A. fumigatus* showed a significant increase in glycerol and trehalose contents. However, the Δ*schA* mutant strain does not increase as much as the wild type the glycerol content and shows significant increased trehalose levels than the wild-type strain. The reduced glycerol levels in the Δ*schA* mutant are probably related to the observed reduction in the abundance of glycerol-3-phosphate dehydrogenase (GpdA; see Table 3), a key enzyme for glycerol biosynthesis (Saito and Posas, 2012). How SchA can reduce GpdA levels remains to be investigated. These results suggest that TOR and Sch9 homologues in fungi were involved in the osmotic stress response via modulating the HOG pathway.

Additionally, we demonstrated that SchA was important for sphingolipid biosynthesis upon osmotic stress. In *S. cerevisiae* Sch9 has been shown to regulate

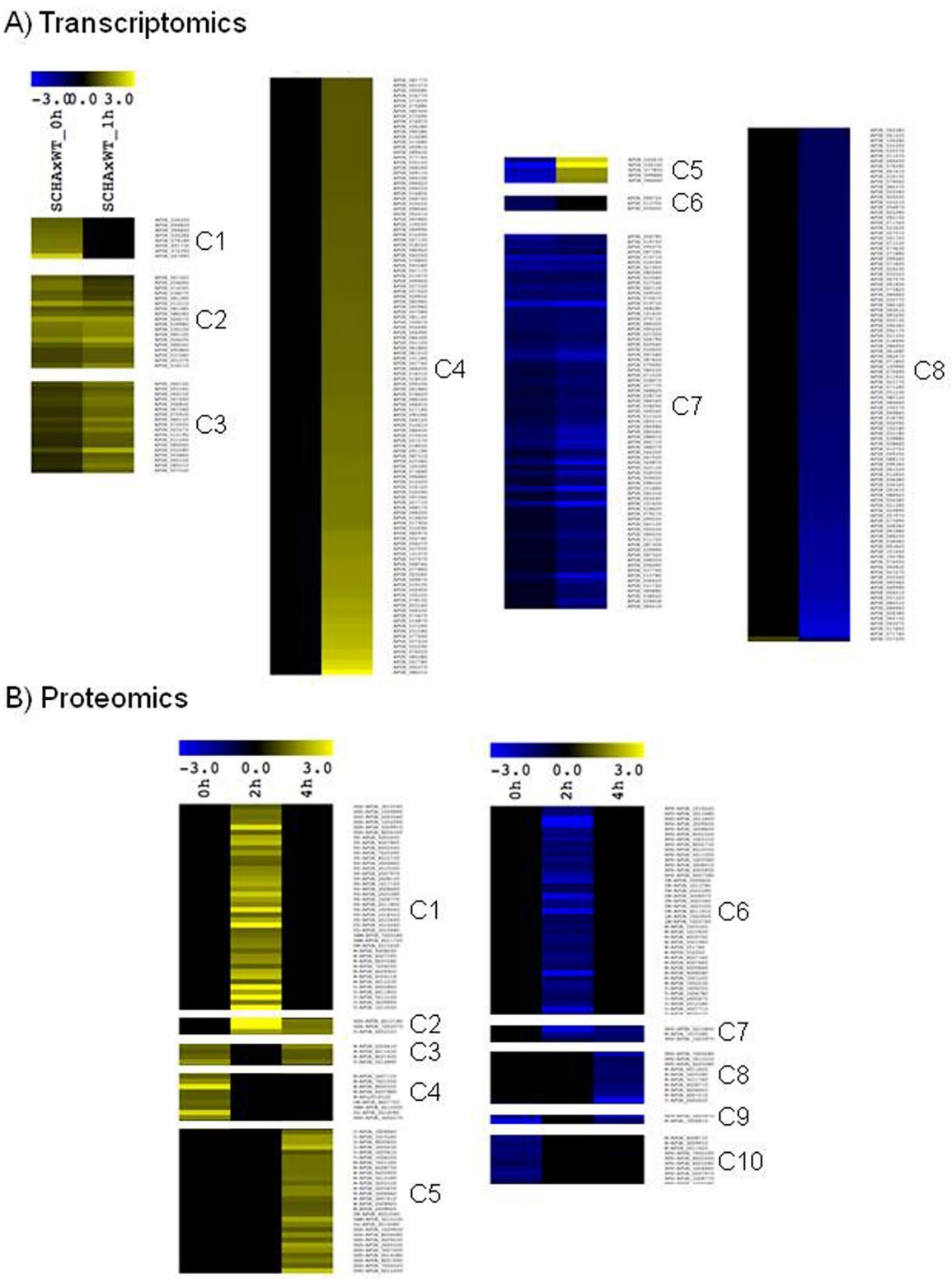

Fig. 9. Cluster analysis of RNA-seq and proteomics data.
A. Analysis of RNAseq data reveals the existence of eight different expression profiles (C1–C8) according to the behavior of the genes with or without exposition to osmotic stress.
B. Cluster Analysis of proteomics data without or with 2 or 4 h of exposition to osmotic stress, revealing the existence of 10 protein-expression profiles (C1–C10). All analyses were performed using hierarchical clustering in MeV software (http://www.tm4.org/mev.html).

sphingolipid signaling (Swinnen *et al*., 2014b). However, there appear to be differences between the two fungal systems, since the *A. fumigatus* Δ*schA* mutant was more sensitive to PHS, while the *sch9*Δ mutant showed increased sensitivity to different inhibitors of sphingolipid metabolism, such as myriocin and aureobasidin A. Nonetheless, both mutants showed decreased levels of several species of (phyto)ceramides, and altered ratios of complex sphingolipids. Lipid rafts or membrane microdomains are comprised by sphingolipids and sterols (Lingwood and Simons, 2010). Lipid rafts can play signal transduction regulatory roles through modifications of the membrane structure that also can affect protein–protein interactions (Douglas and Konopka, 2014;.Farnoud *et al*., 2015). Tanigawa *et al*. (2012) have isolated a *S. cerevisiae* mutant that has constitutive activity of the HOG pathway independently of the osmotic conditions. This mutation was localized in the *LCB2* gene (encoding a subunit of the serine palmitoyltransferase complex, SPT, Fig. 8). Subsequently, the depletion of sphingolipids was shown to activate the HOG pathway. These authors have shown that Sln1 and Sho1 were present in raft enriched detergent-resistant membranes (DRMs). Interestingly, the combination of reduced sphingolipids with osmotic stress causes a separation of Sln1 and increased union of Sho1 with DRMs. These results strongly indicate that SchA and Sch9 are important regulators of sphingolipid biosynthesis, but they have different mechanisms of action. This raises the interesting hypothesis that lipid rafts are important for the mechanisms of sensing osmotic alterations (HOG pathway-mediated) and that translocation of osmosensors may be an essential step in osmosensing.

The *A. fumigatus* osmotic stress, HOG, pathway is composed of two signaling modules: (i) the two-component system (TCS)-like phosphorelay module composed of a hybrid sensor kinase (TcsC/NikA), a histidine-containing phosphotransfer protein (YpdA) and a response regulator (SskA), and (ii) the MAP kinase module comprising of a MAP kinase kinase kinase (MAPKKK, SskB), a MAP kinase kinase (MAPKK, PbsB) and a MAP kinase (MAPK, SakA). The TCS senses and relays environmental signals that subsequently activate the Hog1 MAPK pathway, which mediates the cellular response (Bahn, 2008; Ma *et al*., 2008; Hagiwara *et al*., 2013). Limited information is available about the putative osmosensors, such as Sln1 and Sho1 homologues (Yang *et al*., 2011; Hagiwara *et al*., 2013). Hence, the increased activation of the *A. fumigatus* $SakA^{HOG1}$ in Δ*schA* may potentially be caused by a reduction in sphingolipids.

We demonstrated that SchA contributes to the phosphorylation of the Rps6 ribosomal protein when TOR was activated. The Δ*schA* mutant had a lower Rps6-P/Rps6 ratio than the wild-type strain when exposed to rapamycin or osmotic stress, suggesting that SchA was important for Rps6 phosphorylation. Interestingly, iron excess and starvation increased the ratio Rps6-P/Rps6 in the wild-type. In contrast, upon iron excess and starvation there is a decrease of the Rps6-P/Rps6 ratio in the Δ*schA* mutant when compared to the wild-type strain, strongly indicating that SchA was important for iron assimilation in *A. fumigatus*. Accordingly, Baldin *et al*. (2015) have shown that TOR signaling participates in the regulation of biosynthesis of ornithine, a major precursor of siderophores in *A. fumigatus*. Interestingly, our work revealed that SchA was important for the modulation of ornithine production and amino acid biosynthesis. In addition, *schA* expression increased upon iron starvation and excess, but it was dependent on both HapX and SreA during iron starvation, suggesting that SchA could play a role in the regulation of these two transcription factors during iron starvation. This was emphasized by the fact that both *sidA* and *hapX*, important for iron starvation, had increased expression in the Δ*schA* mutant during iron starvation.

SchA was important for *A. fumigatus* virulence. Other fungal Sch9 homologues are important for virulence in other human and plant pathogens. The *Cryptococcus neoformans* Sch9 null mutant has cells with enlarged capsules, increased thermal tolerance, and it is attenuated in mating and in virulence (Wang *et al*., 2004). The *C. albicans* CaSch9 deletion has no chlamydospores (Nobile *et al*., 2003), reduced cell size, showed a delayed log-phase growth, was sensitive to rapamycin, caffeine and sodium dodecyl sulfate, has reduced filamentation and attenuated virulence in a mouse model of systemic candidiasis (Liu *et al*., 2010). Interestingly, CaSch9 prevented hyphal formation, specifically under hypoxia, and was hyperfilamentous under concomitant hypoxia ($<$10% O_2) and elevated CO_2 levels ($>$1%) at temperatures lower than 37°C (Stichternoth *et al*., 2011). Recently, a novel role for *C. albicans* Sch9 in genetic stability was reported since deletion of CaSch9 leads to a 150-fold to 750-fold increase in chromosome loss (Varshney *et al*., 2015.). In the rice blast fungus *Magnaporthe oryzae*, the ΔMosch9 mutant has defects in conidiation and pathogenesis, producing smaller conidia and appressoria (Chen *et al*., 2014; Gu *et al*., 2015). The *F. graminearum* ΔFgSch9 mutant has reduced production of the mycotoxin deoxynivalenol and was avirulent (Chen *et al*., 2014; Gu *et al*., 2015). Taken together, these studies indicate that Sch9 homologues play an important role in virulence and pathogenicity in different fungal pathogens of plants and animals.

We proposed a possible model for the interaction between *A. fumigatus* SchA, calcineurin-CrzA, and SakA/MpkC during nutrient sensing and osmotic stress (Fig. 12). In *A. fumigatus*, TOR phosphorylates SchA

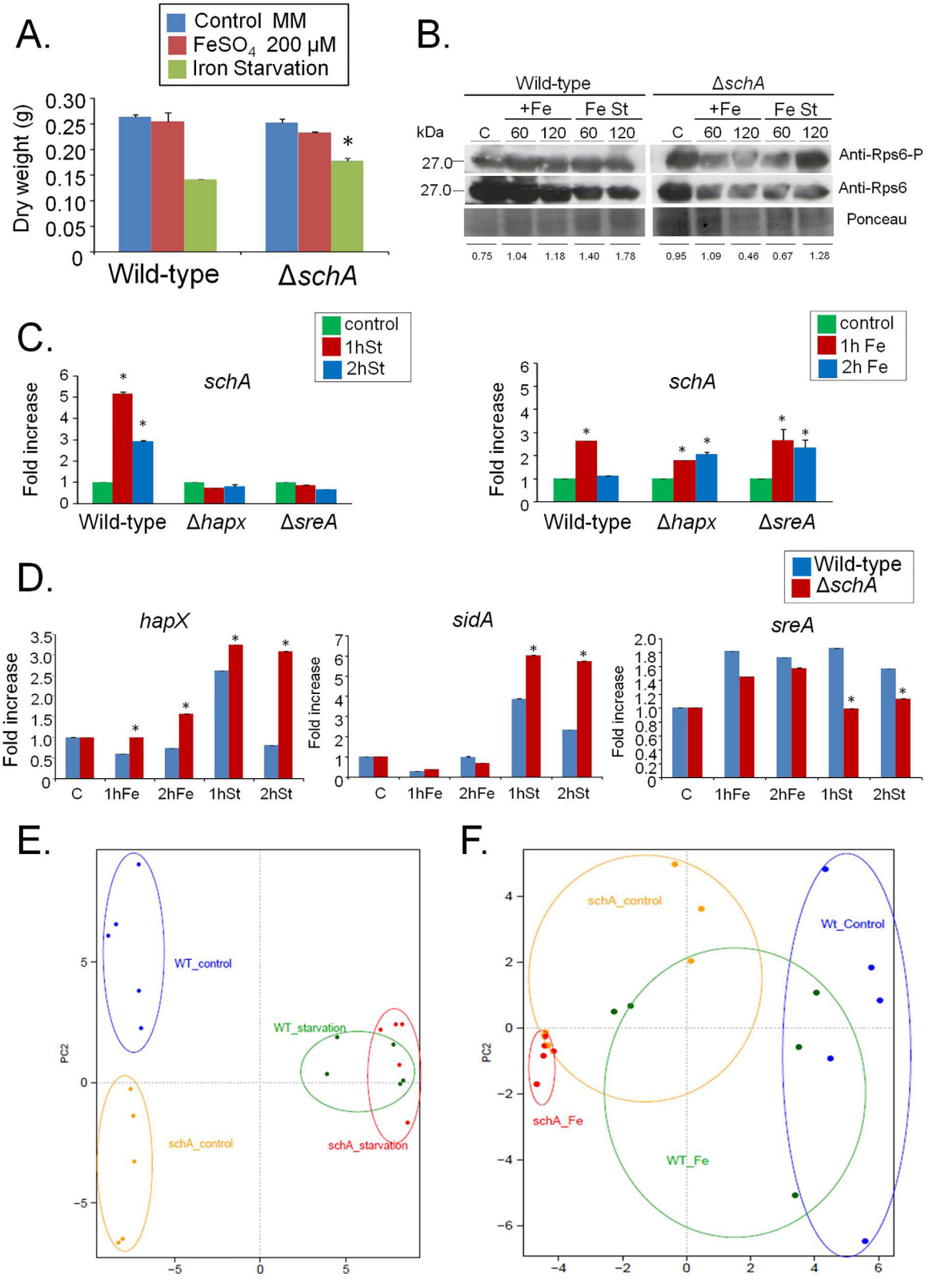
A.
Control MM
FeSO4 200 µM
Iron Starvation
Dry weight (g)
Wild-type
ΔschA
B.
Wild-type
ΔschA
+Fe
Fe St
kDa
C 60 120 60 120
27.0
Anti-Rps6-P
Anti-Rps6
Ponceau
0.75 1.04 1.18 1.40 1.78
0.95 1.09 0.46 0.67 1.28
C.
control
1hSt
2hSt
schA
Fold increase
Wild-type ΔhapX ΔsreA
control
1h Fe
2h Fe
D.
Wild-type
ΔschA
hapX
sidA
sreA
C 1hFe 2hFe 1hSt 2hSt
E.
WT_control
WT_starvation
schA_control
schA_starvation
PC2
F.
schA_control
Wt_Control
schA_Fe
WT_Fe

Fig. 10. *A. fumigatus* SchA is involved in iron metabolism.
A. The wild-type and Δ*schA* mutant strains were grown for 48 h in MM, MM + 200 μM $FeSO_4$ or AMM + 300 μM ferrozine (*, $p < 0.01$, Wild-type compared to Δ*schA*).
B. Western blot analysis for the *A. fumigatus* total and phosphorylated Rps6A. The wild-type and Δ*schA* strains were grown for 20 h at 37°C and exposed or not iron excess or starvation (60 or 120 min) and total proteins extracted. Proteins were normalized by Ponceau red staining. Signal intensities were quantified using the Image J software by dividing the intensity of SakA-P/SakA ratio and expressed as fold increase from the control (0 min).
C. RTqPCR for the *A. fumigatus schA* gene. The strains were grown for 20 h at 37°C and transferred for iron excess or starvation conditions for 1 and 2 h. The results are expressed as fold increase of the control (in the absence of iron excess or starvation) and the results were normalized with the *tubC* expression.
D. RTqPCR for the *A. fumigatus hapX*, *sidA*, and *sreA* genes. The strains were grown for 20 h at 37°C and transferred for iron excess or starvation conditions for 1 and 2 h. The results are expressed as fold increase of the control (in the absence of iron excess or starvation) and the results were normalized with the *tubC* expression.
E and F. Principal Component analysis (PCA) of the gas chromatography study for the wild-type and Δ*schA* strains during iron starvation (left panel) and excess (right panel).

and Rps6 SchA during nutrient sensing or osmotic stress. SchA also phosphorylates Rps6 and other targets, and activates unknown transcription factors which are transported to the nucleus, where they activate targets related to ribosome biogenesis, iron assimilation, ornithine, amino acid biosynthesis, osmotic stress response and sphingolipid biosynthesis. Muñoz *et al.* (2015) showed that hyper-osmotic shock significantly impacted the maximal cytoplasmic (Ca^{2+}) amplitude. Accordingly, the Ca^{2+}-chelator BAPTA inhibited the initial responses to hyperosmotic stress. CrzA goes to the nucleus during osmotic stress and the activity of SakA MAPK is dependent on CrzA (de Castro *et al.*, 2014). This implies that upon osmotic stress, there was an increase in cytoplasmic Ca^{+2}, activating the calcineurin complex that will dephosphorylate the transcription factor CrzA. Then CrzA will be transported to the nucleus to activate genes including the MAP kinases of the HOG/SakA pathway and proteins of the two-component system (TCS). It is not known if there is any interaction between TOR and calcineurin/CrzA. The MAPK SakA and MpkC are controlled by TOR and will be translocated to the nucleus upon nutrient sensing or osmotic stress.

In conclusion, this study revealed novel functions for the *A. fumigatus* SchA, suggesting its involvement with several cell functions and virulence. Novel SchA functions described here are: (i) the connection with calcium metabolism and Ca^{+2}-calcineurin/CrzA pathway, (ii) its involvement with iron assimilation; and (iii) its influence on Rps6p phosphorylation upon several kinds of stress. We have also shown here the first analysis of the influence of a Sch9 homologue in a filamentous fungus on global transcriptomics, proteomics and metabolomics during osmotic stress. In addition, evidences linking the HOG and sphingolipid biosynthesis pathways were also presented. Importantly, we propose that SchA and other Sch9p homologues could serve as mediators of the TOR and HOG pathways. Further studies are necessary to fully understand biochemical interaction and how these two pathways crosstalk during a response to different environmental stresses and pathogenicity. In *A. fumigatus*, both the HOG and calcium-calcineurin/CrzA pathways are important to stress responses and virulence in a mammalian host. Therefore, the identification of the link between these central pathways and TOR will provide new avenues for research into the identification of novel targets for disease intervention.

Experimental procedures

Ethics statement

The principles that guide our studies are based on the Declaration of Animal Rights ratified by the UNESCO in January 27, 1978 in its 8th and 14th articles. All protocols used in this study were approved by the local ethics committee for animal experiments from the Campus of Ribeirão Preto, Universidade de São Paulo (Permit Number: 08.1.1277.53.6; Studies on the interaction of *A. fumigatus* with animals). All animals were housed in groups of five within individually ventilated cages and were cared for in strict accordance with the principles outlined by the Brazilian College of Animal Experimentation (Princípios Éticos na Experimentação Animal – Colégio Brasileiro de Experimentação Animal, COBEA) and Guiding Principles for Research Involving Animals and Human Beings, American Physiological Society. All efforts were made to minimize suffering. Animals were clinically monitored at least twice daily and humanely sacrificed if moribund (defined by lethargy, dyspnoea, hypothermia and weight loss). All stressed animals were sacrificed by cervical dislocation.

Strains, media and culture methods

The *A. fumigatus* parental recipient strains used in this study were Afs35 (FGSC A1159), CEA17 (pyrG+) *akuB*^{KU80} and CEA17(pyrG^{-}) *akuB*^{KU80} (da Silva Ferreira *et al.*, 2006). The mutant strains were: Δ*mpkC*, Δ*sakA*, Δ*mpkC* Δ*sakA*, Δ*mpkC::mpkC*$^{+}$, Δ*sakA::sakA*$^{+}$, SakA::GFP and MpkC::GFP (Hagiwara *et al.*, 2014; Bruder Nascimento *et al.*, 2016). The media used were: complete media composed for 2% w/v glucose, 0.5% w/v yeast extract, trace elements (YAG) and minimal media (MM) consisting of 1% glucose, trace elements and salt solution (Kafer, 1977), pH 6.5, plus or minus 2% w/v agar or AMM, with the same

Table 5. Comparison of the metabolite profile of the wild-type and Δ*schA* mutant strains during growth in iron starvation conditions by GC-MS analysis between. Fold change was built by comparing a given genotype under starvation and control condition and the significant differences were assessed by paired *t*-test.

	Δ*schA* Starvation		Wild-type Starvation	
Compounds	**Fold**	***p*-value**	**Fold**	***p*-value**
Alanine	0.65	0. 00	−0.01	0.93
Aspartate	−4.81	0.00	−3.26	0.00
b-Alanine	−1.20	0.06	−1.20	0.00
Glutamate	NA	NA	0.52	0.02
Glutamine	−1.43	0.01	−0.11	0.78
Glycine	−1.59	0.00	−0.73	0.01
Histidine	−2.47	0.00	−0.17	0.59
Isoleucine	−1.26	0.00	−0.82	0.02
Leucine	−1.21	0.00	−0.54	0.08
Lysine	−2.09	0.00	−0.99	0.00
Methionine	−0.72	NA	NA	NA
Proline	−1.48	0.00	−1.40	0.00
Serine	−1.12	0.00	−0.63	0.02
Tryptophan	−2.97	0.00	−1.17	0.00
Tyrosine	−2.69	0.00	−0.62	0.06
Ornithine	1.35	0.01	−0.41	0.27
Threonine	−1.46	0.00	−0.76	0.02
Putrescine	0.01	0.99	3.15	NA
Urea	−1.35	0.00	−0.65	0.00
(rlz) Spermidine	1.16	0.05	1.45	0.00
Glycerate	0.48	0.14	0.62	0.01
Glycerol	0.37	0.31	0.98	0.02
Pyruvate	2.87	0.00	1.70	0.00
Citrate	−0.26	0.36	1.38	0.00
Isocitrate	2.78	0.00	4.42	0.00
Succinate	2.56	0.00	0.47	0.02
C4H4O4 (Fumarate|Maleate)	−1.23	0.01	−1.31	0.00
Malate	1.36	0.01	0.45	0.09
Pantothenate	2.43	0.00	3.09	NA
(rlx) C5H10O5 (Ribose|Ribulose)	NA	NA	0.52	0.10
(rlx) Mannose	2.39	0.00	1.66	0.00
C4H10O4 (Erythritol|Threitol)	NA	NA	NA	NA
C6H12O5 (Fucose|Epifucose)	−0.27	0.76	−2.60	0.02
Fructose (lPsicose)	6.79	0.00	4.75	0.00
Galactinol	0.29	0.24	−0.02	0.95
Galactitol	4.08	0.00	6.44	0.00
Glucose	7.11	0.00	7.04	0.00
Trehalose	1.07	0.00	0.18	0.61
Melibiose	0.78	0.00	1.37	0.08
Myo-Inositol	−0.84	0.00	−0.07	0.83
Similar to 2-Aminobutyrate	−1.16	0.00	−0.82	0.00
Similar to 2-Hydroxypyridine	1.16	0.07	0.96	0.00

Table 6. Comparison of the metabolite profile of the wild-type and Δ*schA* mutant strains during growth in iron excess conditions by GC-MS analysis between. Fold change was built by comparing a given genotype under iron excess and control condition and the significant differences were assessed by paired t-test.

	Δ*schA*_Fe excess		Wild-type Fe excess	
Compounds	**Fold**	***p*-value**	**Fold**	***p*-value**
Alanine	−0.44	0.03	−0.35	0.02
b-Alanine	0.87	0.09	0.77	0.02
Glutamine	0.05	0.87	1.05	0.02
Histidine	0.78	0.07	1.29	0.01
Methionine	0.34	0.00	NA	NA
Serine	0.53	0.02	0.44	0.06
Tyrosine	0.41	0.07	1.05	0.05
Ornithine	0.67	0.03	−0.75	0.09
Threonine	0.43	0.01	0.60	0.04
Urea	−0.71	0.04	−0.99	0.04
cis-Aconitate	−0.77	0.01	−0.56	0.07
Citrate	0.13	0.56	0.42	0.04
Malate	−2.13	0.00	−0.68	0.22
Ribonate	0.44	0.05	NA	NA
Pantothenate	−0.18	0.33	0.43	0.03
Fructose (lPsicose)	−0.38	0.10	−0.84	0.01
Galactinol	−0.55	0.03	−0.41	0.17
Trehalose	0.27	0.34	−0.83	0.01
Myo-Inositol	−0.65	0.02	−0.39	0.09

concentration of MM, but without iron. Strains were generally grown at 37°C. The pharmacological inhibition of *A. fumigatus* with rapamycin was perfomed by inoculating 1×10^6 conidia in 1 ml of liquid YG media in 24 well polystyrene plates containing 10% Alamar Blue (Life Technologies) as the viability indicator, according to Yamaguchi *et al.* (2002). Cells were grown for 48 h at 37°C and growth assessed at 24 h intervals.

Glycerol and trehalose measurements in mycelia

A. fumigatus conidia (1.0×10^5 to 1.0×10^6) were inoculated into liquid YPD (1% yeast extract, 1% polypeptone and 1% glucose) and cultured for 16 h prior to addition of 1/2 vol. 3 M sorbitol (Final concentration: 1 M) and incubated at 37°C for different periods of time. Mycelia were ground in liquid nitrogen and immediately resuspended by inversion in extraction buffer [50 mM: Tris base pH 7.0, 50 mM NaF, 1 mM Na_3VO_4, 1 mM DTT, phosphatase inhibitor cocktail P0044 (Sigma) and an EDTA-free protease inhibitor cocktail (Roche)] prior to centrifugation for 5 min at 14,000*g*. The protein concentration of the extracts was measured using the Bio-Rad protein assay according to manufacturer's instructions. The glycerol and trehalose content within the extracted cell lysate (equivalent to 5, 10 and 20 μg of total protein for the respective assays) was measured using the Free Glycerol Detection ab65337 kit (AbCam) according to the manufacturer's instructions. The trehalose content was measured using Trehalose Assay kit K-TREH 11/12 (Megazyme) according to the manufacturer's instructions with an additional standard curve ranging from 0 to 4 μg of trehalose dihydrate.

Microscopy

For microscopy, SakA::GFP, or MpkC::GFP conidiospores were grown on coverslips in 4 ml of MM media for 16 h at 30°C. After incubation, the coverslips with adherent germlings were left untreated or treated with 1M sorbitol, 2 ug/ml of rapamycin, iron starvation or excess. Subsequently, the coverslips were rinsed with phosphate-buffered saline (PBS; 140 mM NaCl, 2 mM KCl, 10 mM $NaHPO_4$, 1.8 mM KH_2PO_4, pH7.4) and mounted for examination. Slides were visualized on an Observer Z1 fluorescence microscope

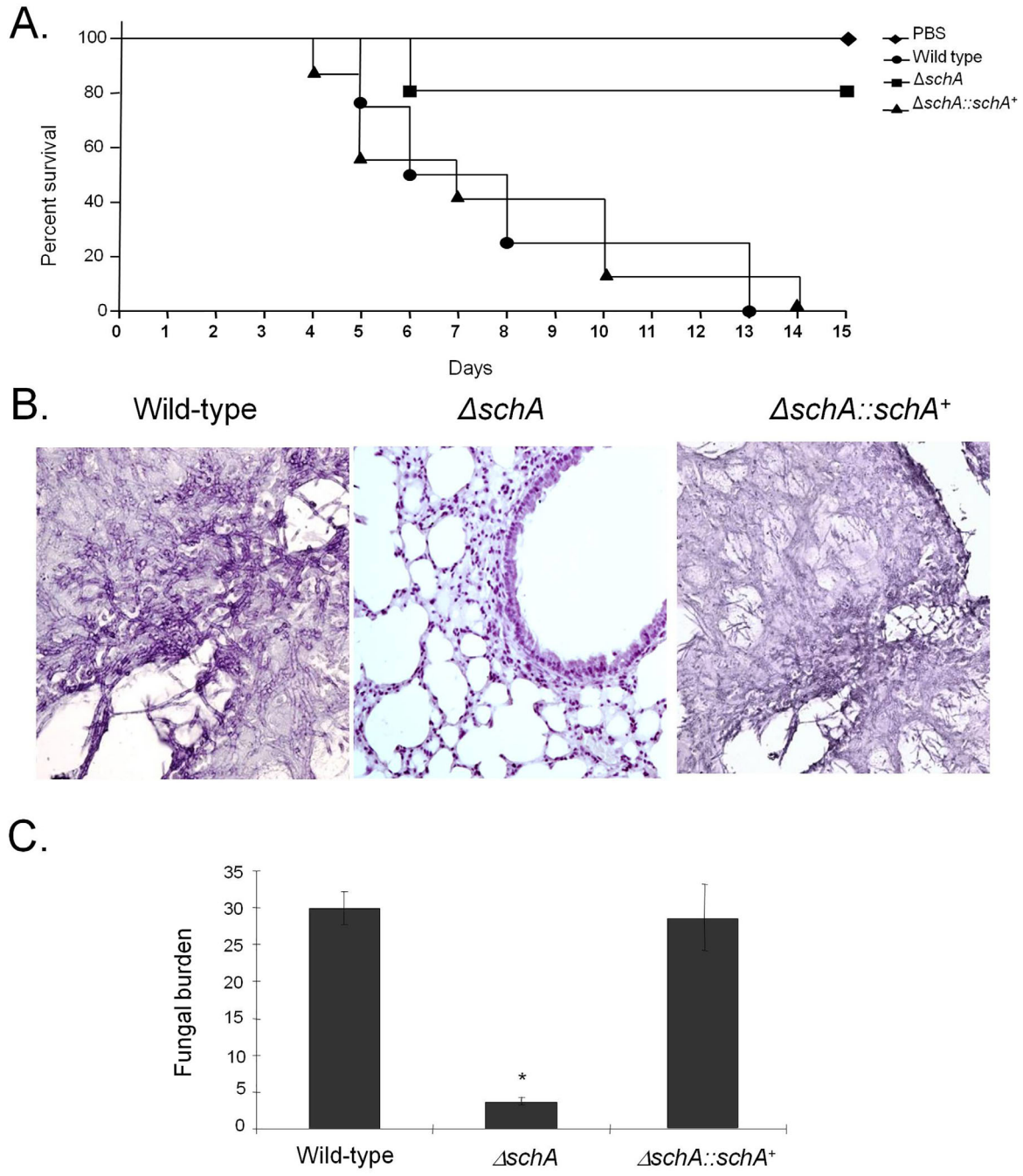

Fig. 11. *A. fumigatus schA* contributes to virulence in neutropenic mice.
A. Comparative analysis of wild-type and the mutants strains in a neutropenic murine model of pulmonary aspergillosis. Mice in groups of 10 per strain were infected intranasally with a 20 μl suspension of conidia at a dose of 10^5.
B. Histological analyses of infection murine lung were performed 72 h after infection (C) Fungal burden was determined 72 h post infection by qPCR based on 18S rRNA gene of *A. fumigatus* and an intronic region of the mouse GAPDH gene.

using a 100x objective oil immersion lens for GFP, filter set 38-high efficiency (HE), excitation wavelength of 450 to 490 nm and emission wavelength of 500 to 550 nm. DIC (differential interference contrast) images and fluorescent images were captured with an AxioCam camera (Carl Zeiss) and processed using AxioVision software (version 4.8).

Construction of the A. fumigatus *mutants*

The gene replacement cassettes were constructed by '*in vivo'* recombination in *S. cerevisiae* as previously described by Colot *et al.* (2006). Thus, approximately 2.0 kb from the 5'-UTR and 3'-UTR flanking region of the targeted ORF regions were selected for primer design. The primers 5F

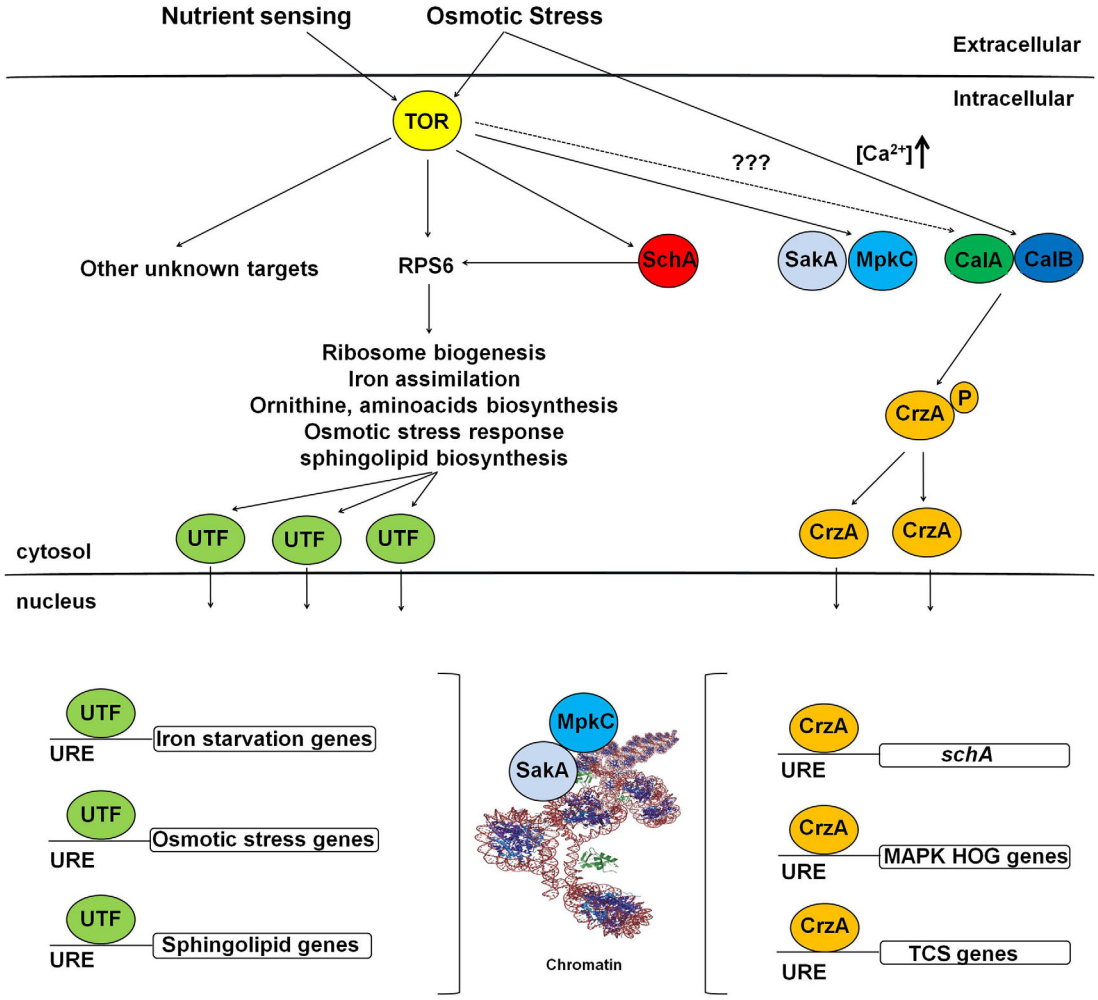

Fig. 12. A possible model for the interaction between *A. fumigatus* SchA, calcineurin/CrzA and SakA/MpkC during nutrient sensing and osmotic stress. *A. fumigatus* TOR phosphorylates SchA and Rps6 SchA during nutrient sensing or osmotic stress. SchA also phosphorylates Rps6 and other targets, and activates unknown transcription factors (UTF). UTFs will be transported to the nucleus via importins and bind to upstream regulatory elements (URE), activating targets related to ribosome biogenesis, iron assimilation, ornithine, amino acids biosynthesis, osmotic stress response and sphingolipids biosynthesis. Upon osmotic stress, there is an increased (Ca^{+2}) released in the cytoplasm, activating the calcineurin complex (CalA and CalB are the catalytic and regulatory subunits respectively) that will dephosphorylate the transcription factor CrzA. CrzA will be transported to the nucleus via importins and bind to UREs, activating genes encoding MAP kinases of the HOG/SakA pathway and proteins of the two-component system (TCS). Upon increased (Ca^{+2}), CrzA binds to the *schA* URE activating transcriptionally this gene. It is not known if there is any interaction between TOR and calcineurin/CrzA. The MAPK SakA and MpkC are controlled by TOR and will be translocated to the nucleus upon nutrient sensing or osmotic stress and will interact with the chromatin. It is likely MpkC modulates SakA and both phosphorylate several of the UTFs to activate them as transcription factors.

and 3R contained a short homologous sequence to the MCS of the plasmid pRS426. Both the 5- and 3-UTR fragments were PCR-amplified from *A. fumigatus* genomic DNA (gDNA). The *pyrG* gene placed within the cassette as a prototrophic marker was amplified from pCDA21 plasmid. The deletion cassette was generated by transforming each fragment along with the plasmid pRS426 cut with *Bam*HI/*Eco*RI into the *S. cerevisiae* strain SC94721 using the lithium acetate method (Schiestl and Gietz, 1989.). The DNA from the transformants was extracted by the method described by Goldman *et al.* (2003). The cassette was PCR-amplified from these plasmids utilizing TaKaRa Ex Taq™ DNA Polymerase (Clontech Takara Bio) and used for *A. fumigatus* transformation. Southern blot analyses demonstrated that the transformation cassettes had integrated homologously at the targeted loci. The single gene deletion strains were complemented by co-transforming a DNA fragment (approximately 1 kb from each 5' and 3'- flanking regions plus the ORF) together with the pHATα (Herrera-Estrella *et al.*, 1990) and selecting for hygromycin resistance in MM plates with 250 mg/ml of hygromycin B.

To generate the double Δ*schA* Δ*sakA* and Δ*schA* Δ*mpkC* mutants, plasmids pSH75-sakA::hph and pUC119-mpkc::ptrA that are described previously (Hagiwara *et al.*,

2013, 2014) were used respectively. From these plasmids, marker cassette flanked by 5'- and 3'-flanking regions of the target gene were amplified by primer sets, sakA-U-F/sakA-D-R and mpkC-U-F/mpkC-D-R (Supporting Information Fig. S2). Transformation by each fragment was conducted in the Δ*schA* as a parental strain, from which transformants were selected with hygromycin or pyrithiamine. Targeted replacement of the *sakA* or *mpkC* genes was confirmed by PCR with the genome and by real-time PCR for the absence of its transcript.

Southern blot analysis was used to demonstrate that the cassettes had integrated homologously at the targeted *A. fumigatus schA* locus. Genomic DNA from *A. fumigatus* was extracted by grinding frozen mycelia in liquid nitrogen and genomic DNA was extracted as previously described (Malavazi and Goldman, 2012). Standard techniques for manipulation of DNA were carried out as described (Sambrook and Russell, 2001). For Southern blot analysis, restricted chromosomal DNA fragments were separated on 1% agarose gel and blotted onto Hybond N^+ nylon membranes (GE Healthcare). Probe labeling for detection was performed using (α-^{32}P)dCTP using the Random Primers DNA Labeling System (Life Technologies). Labeled membranes were exposed to X-ray films, which were scanned for image processing. Southern blot schemes are shown in Supporting Information Fig. S2.

Phenotypic assays

The phenotypes of the deletion mutant were evaluated either by radial growth or assessing the initial growth of a droplet of conidia from a serial dilution, at different temperatures, in the presence or absence of oxidative and osmotic stressing agents, and rapamycin. Drop out experiments were performed using 5 μl of a 10-fold dilution series starting at a concentration of 2×10^7 for the wild-type and mutant strain spotted on different media and grown for 48 h at 37°C. Additionally, dry weight experiments were performed by growing different strains for 48 h at 37°C, washing and lyophilizing the mycelia.

Immunoblot analysis

Detection of SakA phosphorylation by Western blotting was performed as described by Hagiwara *et al*. (2013) with some modifications. Briefly, *A. fumigatus* conidia were inoculated into liquid YPD (1% yeast extract, 1% polypeptone and 1% glucose) and cultured for 16 h prior to addition of 1/2 vol. 3 M sorbitol (Final concentration: 1 M). Mycelia were harvested, frozen and ground into a powder in liquid nitrogen, then mixed with protein extraction buffer containing protease inhibitors. The suspension was centrifuged and the supernatant was boiled with an appropriate sample buffer. Proteins were separated with NuPAGE system (Invitrogen) and blotted using iBlot gel transfer system (Invitrogen). To detect SakA and phosphorylated SakA proteins, a rabbit polyclonal IgG antibody against Hog1 y-215 (Santa Cruz Biotechnology, Santa Cruz, CA, USA) and a rabbit polyclonal IgG antibody against dually phophorylated p38 MAPK (Cell Signaling Technology) were used respectively. The ECL Prime Western Blotting Detection System (GE Healthcare) and LAS1000 (FUJIFILM) were used to detect the signal on blotted membranes.

To assess the phosphorylation status of RPS6, fresh harvested conidia (1×10^7) of the wild-type and mutant strain were inoculated in 50 ml of liquid MM at 37°C for 20 h (160 rpm) and after this period, the mycelia were treated with rapamycin (2 μg/ml) for 10, 30 and 60 min, or submitted to iron starvation or iron excess. For iron starvation, the mycelia was transferred to MM without iron plus 3-(2-pyridyl)−5,6-bis(4-phenylsulfonic acid)−1,2,4-triazine (ferrozine)) 300 μM. For iron excess, 200 μM $FeSO_4$ was added. These treatments were performed for 1 and 2 h and then, the mycelia was frozen and ground in liquid nitrogen. For protein extraction, 0.5 ml of lysis buffer (Valiante *et al*., 2009) containing 10% (v/v) glycerol, 50 mM Tris–HCl pH 7.5, 1% (v/v) Triton X-100, 150 mM NaCl, 0.1% (w/v) SDS, 5 mM EDTA, 50 mM sodium fluoride, 5 mM sodium pyrophosphate, 50 mMb-glycerophosphate, 5 mM sodium orthovanadate, 1 mM PMSF and 1X Complete Mini-protease inhibitor (Roche Applied Science) was added to the ground mycelium. Extracts were centrifuged at 20,000*g* for 40 min at 4°C. The supernatants were collected and the protein concentrations were determined using the Bradford method (Bradford, 1976) (BioRad). 50 μg of protein from each sample were resolved in a 12% (w/v) SDS–PAGE and transferred polyvinylidene difluoride (PVDF) membranes using the iBlot® 2 Dry Blotting System (Thermo Scientific™). The phosphorylation state and total RPS6 was examined using Phospho-S6 Ribossomal Protein (Ser235/236) Antibody, Cell Signaling Technologies and Anti-RPS6 antibody ab40820, abcam®, following the manufacturer's instructions using a 1:1000 dilution in TBST buffer (137 mM NaCl, 20 mM Tris, 0.1% Tween-20). Primary antibody was detected using an Anti-rabbit IgG, HRP-linked Antibody #7074 (Cell Signaling Technologies). Chemoluminescent detection was achieved using the Super Signal West Pico Chemiluminescent Substrate (Thermo Scientific™) and the images generated were subjected to densitometric analysis using the ImageJ software (http://rsbweb.nih.gov/ij/index.html). The RPS6 phosphorylated signal was normalized by total RPS6 signal. Signal intensities were quantified using the Image J software by dividing the intensity of SakA-P/SakA ratio and expressed as fold increase from the control (0 min). The Western blots were repeated twice (Supporting Information Fig. SXXX) and a representative blot for each experiment in shown in the manuscript. We have used the p70 S6 kinase control cell extracts (#9203, Cell Signaling, USA) as a control for the antibody recognition of Rps6-P (see Fig. 1D, right panel).

Label-free quantitative proteomics

Wild-type (CEA17) and Δ*schA* ($5x10^7$spores) were grown in darkness in MM for 24 h, 37°C, 200 rpm. Mycelia were transferred to MM plus 1.2 M sorbitol for 2 and 4 h. Each condition was carried out in triplicate. Sorbitol-free control samples were also prepared for each strain. The mycelia

(18 x samples) were harvested with Miracloth, dried between tissue and snap-frozen in liquid nitrogen. The culture supernatants were also collected. The mycelia were ground in liquid nitrogen and suspended in lysis buffer (100 mM Tris-HCl, 50 mM NaCl, 20 mM EDTA, 10% (v/v) Glycerol, 1 mM PMSF, 1 μg/ml pepstatin A pH 7.5). The mycelia were lyzed using the sonication probe and clarified by centrifugation. The resulting clarified lysates were precipitated using TCA/acetone and resuspended in 8M Urea. Samples were reduced (DTT) and alkylated (IAA) prior to digestion with sequencing grade trypsin combined with ProteaseMax surfactant. Samples were acidified following overnight digestion and the peptide samples were cleaned using C18 spin columns. The resultant peptide samples were analyzed on a Q-Exactive mass spectrometer coupled to a Dionex RSLCnano. The gradient ran from 4 to 35% B over 120 min, and data was collected using a Top15 method for MS/MS scans. Data analysis was performed using MaxQuant software, with Andromeda used for database searching and Perseus used to organize the data (Dolan *et al*., 2014; Owens *et al*., 2015).

Lipid analysis

For lipid analysis by mass spectrometry, *A. fumigatus* conidia from YPG (1% yeast extract, 1% polypeptone and 1% glucose) agar plates were inoculated into liquid YPD media and cultured for 16 h at 37°C. Sorbitol was added, at a final concentration of 1 M, to the separate 16 h grown cultures and grown further for 1 h at 37°C. Then, fungal mass was harvested and lipids extracted (Bligh and Dyer, 1959; Mandala *et al*., 1995). Lipids C17 ceramide and C17 sphingosine were added as internal standards. One tenth of each sample was aliquoted for determination of the inorganic phosphate (Pi). For Pi measurement, 0.6 ml of ashing buffer (10 N H_2SO_4: 10% perchloric acid: water 9:1:40/v:v:v) was added to each sample and heated at 150 °C overnight. Samples were cooled and 0.9 ml of ultrapure water was added. Then, 0.5 ml of 0.9% ammonium molybdate and 0.2 ml of 9% ascorbic acid solution were added to each sample, and incubated at 45 °C for 30 min. Pi amounts for each sample was determined using a sodium dihydrogen phosphate standard curve. Readings were noted at OD_{820} nm.

The remainder of the sample was subjected to base hydrolysis. Briefly, sample was dissolved in 0.5 ml of chloroform and followed by addition of 0.5 ml 0.6 M potassium hydroxide (in methanol). Samples were vortexed and kept at room temperature for 1 h. Samples were then acidified by adding 0.325 ml 1M HCl and 0.125 ml of ultrapure water was added, the tubes vortexed and centrifuged at 3.000 rpm for 10 min. The lower organic phase was transferred to a new tube, dried in SpeedVac, flushed with N_2 and stored at −20°C until analyzed.

The dry lipid extracts were suspended in a buffer containing 1mM ammonium formate + 0.2% fromic acid in methanol (Buffer B) and analyzed using LC-ESI-MS/MS (Liquid chromatography electrospray ionization tandem mass spectrometry) using TSQ Quantum Ultra™ Triple Quadrupole Mass Spectrometer (Thermo Scientific, US). Lipid species were detected by multiple reaction monitoring (MRM) approach described previously (Weckwerth *et al*., 2004; Cuadros-Inostroza *et al*., 2009; Singh *et al*., 2012). A 10 μl sample was delivered by Accela Pump/Autosampler (Thermo Finnigan, US) to the HPLC fitted with 3 μm C8SR, 150 × 3.0 mm column (Peeke Scientific, US). A two buffer mobile system was used: 2mM ammonium formate + 0.2% formic acid in H_2O (Buffer A) and Buffer B. Processing of the collected data was performed using Xcaliber and LCquan software systems. Quantitation of lipid species was based on internal standard normalization using linear regression model as described previously (Bligh and Dyer, 1959; Mandala *et al*., 1995; Bielawski *et al*., 2006). The levels of different lipid species in each sample were normalized to the inorganic phosphate level.

Metabolite profiling analysis

For the metabolite extraction at least five biological replicates were ground to a fine powder. 5 mg of lyophilized material was grounded and extracted in 1 ml of a precooled (−15°C) MTBE: methanol:water 3:1:1 (v/v/v) (Giavalisco *et al*., 2011). 100 μl of the organic phase was dried and derivatized (89). 1 μl of the derivatized samples were analyzed on an Combi-PAL autosampler (Agilent Technologies) coupled to an Agilent 7890 gas chromatograph coupled to a Leco Pegasus 2 time-of-flight mass spectrometer (LECO) as described by Weckwerth *et al*. (2004). Chromatograms were exported from Leco ChromaTOF software (version 3.25) to R software. Peak detection, retention time alignment and library matching were performed using Target Search R-package (Cuadros-Inostroza *et al*., 2009).

Metabolites were quantified by the peak intensity of a selective mass. Metabolites intensities were normalized according to the dried-weight, followed by the sum of total ion count and log 2 transformed. The principal component analysis was performed using pcaMethods bioconductor package (Stacklies *et al*., 2007).

RNA extraction and real-time PCR reactions

Post treatment, mycelia were harvested by filtration, washed twice with H_2O and immediately frozen in liquid nitrogen. For total RNA isolation, mycelia were ground in liquid nitrogen. Total RNA was extracted using Trizol (Invitrogen). The RNA from each treatment was analyzed using an Agilent 2100 Bioanalyzer system to assess the integrity of the RNA. For real-time PCR experiments, RNase free DNase I treatment was carried out as previously described by Semighini *et al*. (2002). Twenty micrograms of total RNA was treated with DNase, purified using a RNAeasy kit (Qiagen) and cDNA was generated using the SuperScript III First Strand Synthesis system (Invitrogen) with oligo(dT) primers, according to the manufacturer's instructions. All the PCR reactions were performed using an ABI 7500 Fast Real-Time PCR System (Applied Biosystems) and SYBR® Green PCR Master Mix (Applied Biosystems). The primer sets for the analyses are listed in Supporting Information Table S8.

Murine model of pulmonary aspergillosis, lung histopathology and fungal burden

Outbreed female mice (BALB/c strain; body weight, 20–22 g) were housed in vented cages containing five animals. Mice were immunosuppressed with cyclophosphamide (150 mg per kg of body weight), which was administered intraperitoneally on days −4, −1 and 2 prior to and post infection. Hydrocortisonacetate (200mg/kg body weight) was injected subcutaneously on day −3. *A. fumigatus* strains were grown on YAG for 2 days prior to infection. Fresh conidia were harvested in PBS and filtered through a Miracloth (Calbiochem). Conidial suspensions were spun for 5 min at 3,000x *g*, washed three times with PBS, counted using a hemocytometer and resuspended at a concentration of 5.0×10^6 conidia/ml. The viability of the administered inoculum was determined by incubating a serial dilution of the conidia on YAG medium, at 37°C. Mice were anesthetized by halothane inhalation and infected by intranasal instillation of 1.0×10^5 conidia in 20 μl of PBS. As a negative control, a group of five mice received PBS only. Mice were weighed every 24 h from the day of infection and visually inspected twice daily. The statistical significance of the comparative survival values was calculated using log rank analysis and the Prism statistical analysis package.

To investigate fungal burden in murine lungs, mice were immunosuppressed with cyclophosphamide (150 mg/kg of body weight), which was administered intraperitoneally on days −4 and −1, while hydrocortisonacetate was injected subcutaneously (200 mg/kg) on day-3. Five mice per group were intranasally inoculated with 1×10^6 conidia/20 μl of suspension. A higher inoculum, in comparison to the survival experiments, was used to increase fungal DNA detection. Animals were sacrificed 72 h post-infection, and the lungs were harvested and immediately frozen in liquid nitrogen. Samples were homogenized by vortexing with glass beads for 10 min, and DNA was extracted via the phenol-chloroform method. DNA quantity and quality were assessed using a NanoDrop 2000 spectrophotometer (Thermo Scientific). At least 500 μg of total DNA from each sample was used for quantitative real-time PCRs. A primer and a Lux probe (Invitrogen) were used to amplify the 18S rRNA region of *A. fumigatus* (primer, 5'-CTTAAATAGCCCGGTCCGCATT-3'; probe, 5'-CATCACAGACCTGTTATTGCCG-3') and an intronic region of mouse GAPDH (glyceraldehyde-3-phosphate dehydrogenase) (primer, 5'-CGAGGGACTTGGAGGACACAG-3'; probe, 5'-GGGCAAGGCTAAAGGTCAGCG-3'). Six-point standard curves were calculated using serial dilutions of gDNA from all the *A. fumigatus* strains used and the uninfected mouse lung. Fungal and mouse DNA quantities were obtained from the threshold cycle (C_T) values from an appropriate standard curve. Fungal burden was determined as the ratio between picograms of fungal and micrograms of mouse DNA.

For the histopathology, the animals were also sacrificed 72 h post-infection, the lungs were removed and fixed for 24 h in 3.7% formaldehyde–PBS. Samples were washed several times in 70% alcohol before dehydration in a series of alcohol solutions of increasing concentrations. Finally, the samples were diafanized in xylol and embedded in paraffin. For each sample, sequential 5 μm thick sections were collected on glass slides and stained with Gomori methenamine silver (GMS) or hematoxylin and eosin (HE) stain following standard protocols. Briefly, sections were deparaffinized, oxidized with 4% chromic acid, stained with methenamine silver solution, and counterstained with picric acid. For HE staining, sections were deparaffinized and stained first with hematoxylin and then with eosin. All stained slides were immediately washed, preserved with mounting medium, and sealed with a coverslip. Microscopic analyses were done using an Axioplan 2 imaging microscope (Zeiss) at the stated magnifications under bright-field conditions.

RNA sequencing

A. fumigatus conidia (1×10^6 sp/ml) were inoculated into liquid YPD (1% yeast extract, 1% polypeptone and 1% glucose) and cultured for 16 h prior to addition of 1/2 vol. 3 M sorbitol (Final concentration: 1 M). Mycelia were harvested, frozen in liquid nitrogen. For total RNA isolation, mycelia were ground in liquid nitrogen. Total RNA was extracted using Trizol (Invitrogen), treated with RNase-free DNase I (Fermentas) and purified using a RNAeasy Kit (Qiagen) according to manufacturer's instructions. The RNA from each treatment was quantified using a NanoDrop and Qubit fluorometer, and analyzed using an Agilent 2100 Bioanalyzer system to assess the integrity of the RNA. RNA Integrity Number (RIN) was calculated; RNA sample had a RIN = 9.0 − 9.5.

Illumina TruSeq Stranded mRNA Sample Preparation kit was used. Briefly, polyA containing mRNA molecules were selected using polyT oligo-attached magnetic beads. Fragmentation and paired-end library preparation was done using divalent cations and thermal fragmentation. First strand cDNA synthesis was performed using reverse transcriptase (Superscript II) and random primers. This was followed by second strand cDNA synthesis using DNA Polymerase I and RNase H and dUTP in place of dTTP. AMPure XP beads were used to separate the dscDNA from the second strand. At the end of this process, we had blunt-ended cDNA to which a single 'A' nucleotide was added at the 3' end to prevent them from ligating to one another during the adapter ligation reaction. A corresponding single 'T' nucleotide on the 3' end of the adapter provided a complementary overhang for ligating the adapter to the fragment. The products were then purified and enriched using a PCR to selectively enrich those DNA fragments that have adapter molecules on both ends and to amplify the amount of DNA in the library. The PCR was performed with a PCR Primer Cocktail from the Illumina kit that anneals to the ends of the adapters. Libraries were sequenced (2×100bp) on a HiSeq 2500 instrument, sequencing approx. 17.3×10^6 fragments per sample. Short reads were submitted to the NCBI's Short Read Archive under the Bioproject: PRJNA305564.

Obtained fastq files were quality checked with FastQC (http://www.bioinformatics.babraham.ac.uk/projects/fastqc/), and cleaned with Trimmomatic (Bolger *et al*. 2014); quality

trim, adaptor removal and minimum length filtering), finally, ribosomal RNA was removed using SortMeRNA (Kopylova *et al*., 2012). High-quality reads were mapped to the A. fumigatus A1163 genome sequence using Tophat2 (Kim *et al*., 2013) in strand-specific mode. Saturation of sequencing effort was assessed by counting the number of detected exon-exon junction at different subsampling levels of the total high-quality reads, using RSeQC (Wang *et al*., 2012). All samples achieved saturation of known exon-exon junctions. In order to assess transcript abundance exonic reads were counted in a strand-specific way using the Rsubread library (Liao *et al*., 2013) from the Bioconductor suite (Huber *et al*., 2015). Differential gene expression analysis was carried-out in EdgeR (Robinson *et al*., 2010) controlling for a False Discovery Rate of 0.05 (Benjamini *et al*., 2001).

Acknowledgements

We thank Douglas Antonio Alvaredo Paixão for technical support in the RNAseq. S.K.D. is a recipient of an Irish Research Council Embark PhD Fellowship. Quantitative proteomic MS facilities were funded by a competitive award from Science Foundation Ireland (12/RI/2346 (3)). Research exchanges between the laboratories of G.H.G., G.W.J., and S.D. were funded in part by SFI/12/ISCA/2494. We would like to thank the Conselho Nacional de Desenvolvimento Científico e Tecnológico (CNPq) and the Fundação de Amparo à Pesquisa do Estado de São Paulo (FAPESP) for providing financial support. S.K.D. is a recipient of an Irish Research Council Embark PhD Fellowship. Quantitative proteomic MS facilities were funded by a competitive award from Science Foundation Ireland (12/RI/2346 (3)). Research exchanges between the laboratories of G.H.G., G.W.J., and S.D. were funded in part by SFI/12/ISCA/2494. We also would like to thank the three anonymous reviewers and the editor for their suggestions and comments.

References

Altwasser, R., Baldin, C., Weber, J., Guthke, R., Kniemeyer, O., *et al*. (2015) Network modeling reveals cross talk of MAP kinases during adaptation to caspofungin stress in *Aspergillus fumigatus*. *PLoS One* **10**: e0136932.

Bahn, Y.S. (2008) Master and commander in fungal pathogens: the two-component system and the HOG signaling pathway. *Eukaryot Cell* **7**: 2017–2036.

Baldin, C., Valiante, V., Krüger, T., Schafferer, L., Haas, H., *et al*. (2015) Comparative proteomics of a tor inducible *Aspergillus fumigatus* mutant reveals involvement of the Tor kinase in iron regulation. *Proteomics* **15**: 2230–2243.

Benjamini, Y., Drai, D., Elmer, G., Kafkafi, N., and Golani, I. (2001) Controlling the false discovery rate in behavior genetics research. *Behav Brain Res* **125**: 279–284.

Bielawski, J., Szulc, Z.M., Hannun, Y.A., and Bielawska, A. (2006) Simultaneous quantitative analysis of bioactive sphingolipids by high-performance liquid chromatography-tandem mass spectrometry. *Methods* **39**: 82–91.

Bligh, E.G., and Dyer, W.J. (1959) A rapid method of total lipid extraction and purification. *Can J Biochem Physiol* **37**: 911–917.

Bolger, A.M., Lohse, M., and Usadel, B. (2014) Trimmomatic: a flexible trimmer for Illumina sequence data. *Bioinformatics* **30**: 2114–2120.

Bradford, M.M. (1976) Rapid and sensitive method for the quantitation of microgram quantities of protein utilizing the principle of protein-dye binding. *Anal Biochem* **72**: 248–254.

Brown, G.D., Denning, D.W., and Levitz, S.M. (2012a) Tackling human fungal infections. *Science* **336**: 647.

Brown, G.D., Denning, D.W., Gow, N.A., Levitz, S.M., Netea, M.G., and White, T.C. (2012b) Hidden killers: human fungal infections. *Sci Transl Med* **4**: 165rv13.

Brown, N.A., de Gouvea, P.F., Krohn, N.G., Savoldi, M., and Goldman, G.H. (2013) Functional characterisation of the non-essential protein kinases and phosphatases regulating *Aspergillus nidulans* hydrolytic enzyme production. *Biotechnol Biofuels* **6**: 91.

Bruder Nascimento, A.C.O., Dos Reis, T.F., de Castro, P.A., Hori, J.I., Bom, V.L., de Assis, L.J., *et al*. (2016) Mitogen activated protein kinases $SakA^{HOG1}$ and MpkC collaborate for *Aspergillus fumigatus* virulence. *Mol Microbiol* **100**: 841–859

de Castro, P.A., Chen, C., de Almeida, R.S., Freitas, F.Z., Bertolini, M.C., Morais, E.R., *et al*. (2014) ChIP-seq reveals a role for CrzA in the *Aspergillus fumigatus* high-osmolarity glycerol response (HOG) signalling pathway. *Mol Microbiol* **94**: 655–674.

Chen, D., Wang, Y., Zhou, X., Wang, Y., and Xu, J.R. (2014) The Sch9 kinase regulates conidium size, stress responses, and pathogenesis in *Fusarium graminearum*. *PLoS One* **9**: e105811.

Colot, H.H., Park, G., Turner, G.E., Ringelberg, C., Crew, C.M., Litvinkova, L., *et al*. (2006) A highthroughput gene knockout procedure for *Neurospora* reveals functions for multiple transcription factors. *Proc Nat Acad Sci USA* **103**: 10352–10357.

Cornu, M., Albert, V., and Hall, M.N. (2013) mTOR in aging, metabolism, and cancer. *Curr Opin Genet Dev* **23**: 53–62.

Cuadros-Inostroza, A., Caldana, C., Redestig, H., Kusano, M., Lisec, J., Peña-Cortés, H., *et al*. (2009) TargetSearch–a Bioconductor package for the efficient preprocessing of GC-MS metabolite profiling data. *BMC Bioinformatics* **10**: 428.

Dagenais, T.R., and Keller, N.P. (2009) Pathogenesis of *Aspergillus fumigatus* in Invasive Aspergillosis. *Clin Microbiol Rev* **22**: 447–465.

Dobrenel, T., Marchive, C., Azzopardi, M., Clément, G., Moreau, M., Sormani, R., *et al*. (2013) Sugar metabolism and the plant target of rapamycin kinase: a sweet operator? *Front Plant Sci* **4**: 93.

Dolan, S.K., Owens, R.A., O'keeffe, G., Hammel, S., Fitzpatrick, D.A., Jones, G.W., *et al*. (2014) Regulation of non-ribosomal peptide synthesis: bis-thiomethylation attenuates gliotoxin biosynthesis in *Aspergillus fumigatus*. *Chem Biol* **21**: 999–1012.

Douglas, L.M., and Konopka, J.B. (2014) Fungal membrane organization: the eisosome concept. *Annu Rev Microbiol* **68**: 377–393.

Fabrizio, P., Pozza, F., Pletcher, S.D., Gendron, C.M., and Longo, V.D. (2001) Regulation of longevity and stress resistance by Sch9 in yeast. *Science* **292**: 288–290.

Farnoud, A.M., Toledo, A.M., Konopka, J.B., Del Poeta, M., and London, E. (2015) Raft-like membrane domains in pathogenic microorganisms. *Curr Top Membr* **75**: 233–268.

Fillinger, S., Chaveroche, M.K., Shimizu, K., Keller, N., and D'enfert, C. (2002) cAMP and ras signalling independently control spore germination in the filamentous fungus *Aspergillus nidulans*. *Mol Microbiol* **44**: 1001–1016.

Fitzgibbon, G.J., Morozov, I.Y., Jones, M.G., and Caddick, M.X. (2005) Genetic analysis of the TOR pathway in *Aspergillus nidulans*. *Eukaryot Cell* **4**: 1595–1598.

Giavalisco, P., Li, Y., Matthes, A., Eckhardt, A., Hubberten, H.M., Hesse, H., *et al*. (2011) Elemental formula annotation of polar and lipophilic metabolites using (13) C, (15) N and (34) S isotope labelling, in combination with high-resolution mass spectrometry. *Plant J* **68**: 364–376.

Goldman, G.H., dos Reis Marques, E., Duarte Ribeiro, D.C., de Souza Bernardes, L.A., Quiapin, A.C., Vitorelli, P.M., *et al*. (2003) Expressed sequence tag analysis of the human pathogen *Paracoccidioides brasiliensis* yeast phase: identification of putative homologues of *Candida albicans* virulence and pathogenicity genes. *Eukaryot Cell* **2**: 34–48.

González, A., Shimobayashi, M., Eisenberg, T., Merle, D.A., Pendl, T., Hall, M.N., *et al*. (2015) TORC1 promotes phosphorylation of ribosomal protein S6 via the AGC kinase Ypk3 in *Saccharomyces cerevisiae*. *PLoS One* **10**: e0120250.

Greenberger, P.A. (2002) Allergic bronchopulmonary aspergillosis. *J Allergy Clin Immunol* **110**: 685–692.

Gsaller, F., Hortschansky, P., Beattie, S.R., Klammer, V., Tuppatsch, K., Lechner, B.E., *et al*. (2014) The Janus transcription factor HapX controls fungal adaptation to both iron starvation and iron Excess. *Embo J* **33**: 2261–2276.

Gu, Q., Zhang, C., Yu, F., Yin, Y., Shim, W.B., and Ma, Z. (2015) Protein kinase FgSch9 serves as a mediator of the target of rapamycin and high osmolarity glycerol pathways and regulates multiple stress responses and secondary metabolism in *Fusarium graminearum*. *Environ Microbiol* **17**: 2661–2676.

Hagiwara, D., Takahashi-Nakaguchi, A., Toyotome, T., Yoshimi, A., Abe, K., Kamei, K., *et al*. (2013) NikA/TcsC histidine kinase is involved in conidiation, hyphal morphology, and responses to osmotic stress and antifungal chemicals in *Aspergillus fumigatus*. *PLoS One* **8**: e80881.

Hagiwara, D., Suzuki, S., Kamei, K., Gonoi, T., and Kawamoto, S. (2014) The role of AtfA and HOG MAPK pathway in stress tolerance in conidia of *Aspergillus fumigatus*. *Fungal Genet Biol* **73**: 138–149.

Heitman, J., Movva, N.R., and Hall, M.N. (1991) Targets for cell cycle arrest by the immunosuppressant rapamycin in yeast. *Science* **253**: 905–909.

Herrera-Estrella, A., Goldman, G.H., and Van Montagu, M. (1990) High-efficiency transformation system for the biocontrol agents, *Trichoderma* spp. *Mol Microbiol* **4**: 839–843.

Huber, W., Carey, V.J., Gentleman, R., Anders, S., Carlson, M., Carvalho, B.S., *et al*. (2015) Orchestrating high-throughput genomic analysis with Bioconductor. *Nat Methods* **12**: 115–121.

Jorgensen, P., Rupes, I., Sharom, J.R., Schneper, L., Broach, J.R., and Tyers, M. (2004) A dynamic transcriptional network communicates growth potential to ribosome synthesis and critical cell size. *Genes Dev* **18**: 2491–2505.

Kafer, E. (1977) Meiotic and mitotic recombination in *Aspergilllus* and its chromosomal aberrations. *Adv Genet* **19**: 33–131.

Kim, D., Pertea, G., Trapnell, C., Pimentel, H., Kelley, R., and Salzberg, S.L. (2013) TopHat2: accurate alignment of transcriptomes in the presence of insertions, deletions and gene fusions. *Genome Biol* **14**: R36.

Kopylova, E., Noé, L., and Touzet, H. (2012) SortMeRNA: fast and accurate filtering of ribosomal RNAs in metatranscriptomic data. *Bioinformatics* **28**: 3211–3217.

Kwon-Chung, K.J., and Sugui, J.A. (2013) *Aspergillus fumigatus* - what makes the species a ubiquitous human fungal pathogen? *PLoS Pathog* **9**: e1003743.

Lackner, M., and Lass-Flörl, C. (2013) Up-date on diagnostic strategies of invasive aspergillosis. *Curr Pharm Des* **19**: 3595–3614.

Laplante, M., and Sabatini, D.M. (2012) mTOR signaling in growth control and disease. *Cell* **149**: 274–293.

Liao, Y., Smyth, G.K., and Shi, W. (2013) The Subread aligner: fast, accurate and scalable read mapping by seed-and-vote. *Nucleic Acids Res* **41**: e108.

Liko, D., and Hall, M.N. (2015) mTOR in health and in sickness. *J Mol Med* **93**: 1061–1073.

Lingwood, D., and Simons, K. (2010) Lipid rafts as a membrane-organizing principle. *Science* **327**: 46–50.

Liu, W., Zhao, J., Li, X., Li, Y., and Jiang, L. (2010) The protein kinase CaSch9p is required for the cell growth, filamentation and virulence in the human fungal pathogen *Candida albicans*. *FEMS Yeast Res* **10**: 462–470.

Loewith, R., Jacinto, E., Wullschleger, S., Lorberg, A., Crespo, J.L., Bonenfant, D., *et al*. (2002) Two TOR complexes, only one of which is rapamycin sensitive, have distinct roles in cell growth control. *Mol Cell* **10**: 457–468.

Longo, V.D., and Fabrizio, P. (2012) Chronological aging in *Saccharomyces cerevisiae*. *Subcell Biochem* **57**: 101–121.

Lopez-Berges, M.S., Rispail, N., Prados-Rosales, R.C., and Di Pietro, A. (2010) A nitrogen response pathway regulates virulence functions in *Fusarium oxysporum* via the protein kinase TOR and the bZIP protein MeaB. *Plant Cell* **22**: 2459–2475.

Lv, X., Zhang, W., Chen, G., and Liu, W. (2015) *Trichoderma reesei* Sch9 and Yak1 regulate vegetative growth, conidiation, and stress response and induced cellulase production. *J Microbiol* **53**: 236–242.

Ma, Y., Qiao, J., Liu, W., Wan, Z., Wang, X., Calderone, R., *et al*. (2008) The sho1 sensor regulates growth, morphology, and oxidant adaptation in *Aspergillus fumigatus* but is not essential for development of invasive pulmonary aspergillosis. *Infect Immun* **76**: 1695–1701.

Maeda, T., Wurgler-Murphy, S.M., and Saito, H. (1994) A two-component system that regulates an osmosensing MAP kinase cascade in yeast. *Nature* **369**: 242–245.

Mandala, S.M., Thornton, R.A., Frommer, B.R., Curotto, J.E., Rozdilsky, W., Kurtz, M.B., *et al*. (1995) The

discovery of australifungin, a novel inhibitor of sphinganine N-acyltransferase from *Sporormiella australis*. Producing organism, fermentation, isolation, and biological activity. *J Antibiot* **48**: 349–356.
May, G.S. (2008) Mitogen-activated protein kinase pathways in Aspergilli. In *The Aspergilli. Genomics, Medical Aspects, Biotechnology, and Research Methods*. Goldman, G.H. and Osmani, S.A. (eds.). Boca Raton, FL, USA: CRC Press, pp. 121–127.
Malavazi, I., and Goldman, G.H. (2012) Gene disruption in *Aspergillus fumigatus* using a PCR-based strategy and in vivo recombination in yeast. *Methods Mol Biol* **845**: 99–118.
Moore, M.M. (2013) The crucial role of iron uptake in *Aspergillus fumigatus* virulence. *Curr Opin Microbiol* **16**: 692–699.
Muñoz, A., Bertuzzi, M., Bettgenhaeuser, J., Iakobachvili, N., Bignell, E.M., and Read, N.D. (2015) Different stress-induced calcium signatures are reported by aequorin-mediated calcium measurements in living cells of *Aspergillus fumigatus*. *PLoS One* **10**: e0138008.
Nakashima, A., Sato, T., and Tamanoi, F. (2010) Fission yeast TORC1 regulates phosphorylation of ribosomal S6 proteins in response to nutrients and its activity is inhibited by rapamycin. *J Cell Sci* **123**: 777–786.
Nobile, C.J., Bruno, V.M., Richard, M.L., Davis, D.A., and Mitchell, A.P. (2003) Genetic control of chlamydospore formation in *Candida albicans*. *Microbiology* **149**(Pt12): 3629–3637.
Owens, R.A., O'keeffe, G., Smith, E.B., Dolan, S.K., Hammel, S., Sheridan, K.J., *et al*. (2015) Interplay between gliotoxin resistance, secretion and the methyl/methionine cycle in *Aspergillus fumigatus*. *Eukaryot Cell* **14**: 941–957.
Pascual-Ahuir, A., and Proft, M. (2007) The Sch9 kinase is a chromatin-associated transcriptional activator of osmostress-responsive Genes. *Embo J* **26**: 3098–3108.
Pearson, G., Robinson, F., Beers Gibson, T., Xu, B.E., Karandikar, M., Berman, K., *et al*. (2001) Mitogen-activated protein (MAP) kinase pathways: regulation and physiological functions. *Endocr Rev* **22**: 153–183.
Powers, T. (2007) TOR signaling and S6 kinase 1: Yeast catches up. *Cell Metab* **6**: 1–2.
Reinke, A., Anderson, S., McCaffery, J.M., Yates, J., 3rd, Aronova, S., Chu, S., *et al*. (2004) TOR complex 1 includes a novelcomponent, Tco89p (YPL180w), and cooperates with Ssd1p to maintain cellular integrity in *Saccharomyces cerevisiae*. *J Biol Chem* **279**: 14752–14762.
Reyes, G., Romans, A., Nguyen, C.K., and May, G.S. (2006) Novel mitogen-activated protein kinase MpkC of *Aspergillus fumigatus* is required for utilization of polyalcohol sugars. *Eukaryot Cell* **5**: 1934–1940.
Rispail, N., Soanes, D.M., Ant, C., Czajkowski, R., Grünler, A., Huguet, R., *et al*. (2009) Comparative genomics of MAP kinase and calcium-calcineurin signalling components in plant and human pathogenic fungi. *Fungal Genet Biol* **46**: 287–298.
Robaglia, C., Thomas, M., and Meyer, C. (2012) Sensing nutrient and energy status by SnRK1 and TOR kinases. *Curr Opin Plant Biol* **15**: 301–307.
Robinson, M.D., McCarthy, D.J., and Smyth, G.K. (2010) edgeR: a Bioconductor package for differential expression analysis of digital gene expression data. *Bioinformatics* **26**: 139–140.
Saito, H., and Posas, F. (2012) Response to hyperosmotic stress. *Genetics* **192**: 289–318.
Sambrook, J., and Russell, D.W. (2001) *Molecular Cloning: A Laboratory Manual*, 3rd edn. London: CSHL Press.
Schiestl, R.H., and Gietz, R.D. (1989) High efficiency transformation of intact yeast cells using single stranded nucleic acids as a carrier. *Curr Genet* **16**: 339–346.
Schrettl, M., and Haas, H. (2011) Iron homeostasis-Achilles' heel of *Aspergillus fumigatus*? *Curr Opin Microbiol* **14**: 400–405.
Semighini, C.P., Marins, M., Goldman, M.H.S., and Goldman, G.H. (2002) Quantitative analysis of the relative transcript levels of ABC transporter *Atr* genes in *Aspergillus nidulans* by real-time reverse transcription-PCR assay. *Appl Environ Microbiol* **68**: 1351–1357.
da Silva Ferreira, M.E., Kress, M.R., Savoldi, M., Goldman, M.H., Hartl, A., Heinekamp, T., *et al*. (2006) The akuB(KU80) mutant deficient for nonhomologous end joining is a powerful tool for analyzing pathogenicity in *Aspergillus fumigatus*. *Eukaryot Cell* **5**: 207–211.
Singh, A., Wang, H., Silva, L.C., Na, C., Prieto, M., Futerman, A.H., *et al*. (2012) Methylation of glycosylated sphingolipid modulates membrane lipid topography and pathogenicity of *Cryptococcus neoformans*. *Cell Microbiol* **14**: 500–516.
Smets, B., Ghillebert, R., De Snijder, P., Binda, M., Swinnen, E., De Virgilio, C., *et al*. (2010) Life in the midst of scarcity: adaptations to nutrient availability in *Saccharomyces cerevisiae*. *Curr Genet* **56**: 1–32.
Soriani, F.M., Malavazi, I., da Silva Ferreira, M.E., Savoldi, M., Von Zeska Kress, M.R., de Souza Goldman, M.H., *et al*. (2008) Functional characterization of the *Aspergillus fumigatus* CRZ1 homologue, CrzA. *Mol Microbiol* **67**: 1274–1291.
Spincemaille, P., Matmati, N., Hannun, Y.A., Cammue, B.P., and Thevissen, K. (2014) Sphingolipids and mitochondrial function in budding yeast. *Biochim Biophys Acta* **1840**: 3131–3137.
Stacklies, W., Redestig, H., Scholz, M., Walther, D., and Selbig, J. (2007) pcaMethods a bioconductor package providing PCA methods for incomplete data. *Bioinformatics* **23**: 1164–1167.
Stichternoth, C., Fraund, A., Setiadi, E., Giasson, L., Vecchiarelli, A., and Ernst, J.F. (2011) Sch9 kinase integrates hypoxia and CO2 sensing to suppress hyphal morphogenesis in Candida albicans. *Eukaryot Cell* **10**: 502–511.
Swinnen, E., Ghillebert, R., Wilms, T., and Winderickx, J. (2014a) Molecular mechanisms linking the evolutionary conserved TORC1-Sch9 nutrient signalling branch to lifespan regulation in *Saccharomyces cerevisiae*. *FEMS Yeast Res* **14**: 17–32.
Swinnen, E., Wilms, T., Idkowiak-Baldys, J., Smets, B., De Snijder, P., Accardo, S., *et al*. (2014b) The protein kinase Sch9 is a key regulator of sphingolipid metabolism in *Saccharomyces cerevisiae*. *Mol Biol Cell* **25**: 196–211.
Tanigawa, M., Kihara, A., Terashima, M., Takahara, T., and Maeda, T. (2012) Sphingolipids regulate the yeast high-osmolarity glycerol response pathway. *Mol Cell Biol* **32**: 2861–2870.

Teichert, S., Wottawa, M., Schonig, B., and Tudzynski, B. (2006) Role of the *Fusarium fujikuroi* TOR kinase in nitrogen regulation and secondary metabolism. *Eukaryot Cell* **5**: 1807–1819.

Tekaia, F., and Latgé, J.P. (2005) *Aspergillus fumigatus*: saprophyte or pathogen? *Curr Opin Microbiol* **8**: 385–392.

Thewes, S. (2014) Calcineurin-Crz1 signaling in lower eukaryotes. *Eukaryot Cell* **13**: 694–705.

Urban, J., Soulard, A., Huber, A., Lippman, S., Mukhopadhyay, D., Deloche, O., *et al*. (2007) Sch9 is a major target of TORC1 in *Saccharomyces cerevisiae*. *Mol Cell* **26**: 663–674.

Valiante, V., Jain, R., Heinekamp, T., and Brakhage, A.A. (2009) The MpkA MAP kinase module regulates cell wall integrity signaling and pyomelanin formation in *Aspergillus fumigatus*. *Fungal Genet Biol* **46**: 909–918.

Valiante, V., Macheleidt, J., Föge, M., and Brakhage, A.A. (2015) The *Aspergillus fumigatus* cell wall integrity signaling pathway: drug target, compensatory pathways, and virulence. *Front Microbiol* **6**: 325.

Varshney, N., Schaekel, A., Singha, R., Chakraborty, T., van Wijlick, L., Ernst, J.F., *et al*. (2015) A surprising role for the Sch9 protein kinase in chromosome segregation in Candida albicans. *Genetics* **199**: 671–674.

Voordeckers, K., Kimpe, M., Haesendonckx, S., Louwet, W Versele, M., and Thevelein, J.M. (2011) Yeast 3-phosphoinositide-dependent protein kinase-1 (PDK1) orthologs Pkh1-3 differentially regulate phosphorylation of protein kinase A (PKA) and the protein kinase B (PKB)/S6K ortholog Sch9. *J Biol Chem* **286**: 22017–22027.

de Vries, R.P., and Visser, J. (2001) *Aspergillus* enzymes involved in degradation of plant cell wall polysaccharides. *Microbiol Mol Biol Rev* **65**: 497–522.

Wang, L., Wang, S., and Li, W. (2012) RSeQC: quality control of RNA-seq experiments. *Bioinformatics* **28**: 2184–2185.

Wang, P., Cox, G.M., and Heitman, J. (2004) A Sch9 protein kinase homologue controlling virulence independently of the cAMP pathway in *Cryptococcus neoformans*. *Curr Genet* **46**: 247–255.

Weckwerth, W., Loureiro, M.E., Wenzel, K., and Fiehn, O. (2004) Differential metabolic networks unravel the effects of silent plant phenotypes. *Proc Natl Acad Sci USA* **101**: 7809–7814.

Winkelströter, L.K., Dolan, S.K., Dos Reis, T.F., Bom, V.L., de Castro, P.A., Hagiwara, D., *et al*. (2015) Systematic global analysis of genes encoding protein phosphatases in *Aspergillus fumigatus*. *G35* **5**: 1525–1539.

Wullschleger, S., Loewith, R., and Hall, M.N. (2006) TOR signaling in growth and metabolism. *Cell* **124**: 471–484.

Wong Sak Hoi, J., Lamarre, C., Beau, R., Meneau, I., Berepiki, A., Barre, A., *et al*. (2011) A novel family of dehydrin-like proteins is involved in stress response in the human fungal pathogen *Aspergillus fumigatus*. *Mol Biol Cell* **22**: 1896–1906.

Yamaguchi, H., Uchid, K., Nagino, K., and Matsunaga, T. (2002) Usefulness of a colorimetric method for testing antifungal drug susceptibilities of *Aspergillus* species to voriconazole. *J Infect Chemother* **8**: 374–377.

Yang, F., Ma, D., Wan, Z., Liu, W., Ji, Y., and Li, R. (2011) The role of sho1 in polarized growth of *Aspergillus fumigatus*. *Mycopathologia* **172**: 347–355.

Yu, F., Gu, Q., Yun, Y., Yin, Y., Xu, J.R., Shim, W.B., *et al*. (2014) The TOR signaling pathway regulates vegetative development and virulence in *Fusarium graminearum*. *New Phytol* **203**: 219–232.

Yuan, H.X., Xiong, Y., and Guan, K.L. (2013) Nutrient sensing, metabolism, and cell growth control. *Mol Cell* **49**: 379–387.

Supporting information

Additional supporting information may be found in the online version of this article at the publisher's web-site.